Shell variability in the stem turtles *Proterochersis* spp.

Tomasz Szczygielski [Corresp., 1, 2] , Justyna Słowiak [1] , Dawid Dróżdż [1]

[1] Department of Evolutionary Paleobiology, Institute of Paleobiology, Polish Academy of Sciences, Warsaw, Poland

[2] Department of Paleobiology and Evolution, Faculty of Biology, Biological and Chemical Research Centre, University of Warsaw, Warsaw, Poland

Corresponding Author: Tomasz Szczygielski
Email address: t.szczygielski@twarda.pan.pl

Background. Turtle shells tend to exhibit frequent and substantial variability, both in bone and scute layout. Aside from secondary changes, caused by diseases, parasites, and trauma, this variability appears to be inherent and result from stochastic or externally-induced flaws of developmental programs. It is, thus, expected to be present in fossil turtle species at least as prominently, as in modern populations. Descriptions of variability and ontogeny are, however, rare for fossil turtles, mainly due to rarity, incompleteness, damage, and post-mortem deformation of their remains. This paper is an attempt at description and interpretation of external shell variability in representatives of the oldest true turtles, *Proterochersis robusta* and *P. porebensis* (Proterochersidae, the sister group to all other known testudinatans) from the Late Triassic (Norian) of Germany and Poland.

Methods. All the available shell remains of *Proterochersis robusta* (13 specimens) and *P. porebensis* (275 specimens) were studied morphologically in order to identify any ontogenetic changes, intraspecific variability, sexual dimorphism, and shell abnormalities. To test the inferred sexual dimorphism, shape analyses were performed for two regions (gular and anal) of the plastron.

Results. *Proterochersis* spp. exhibits large shell variability, and at least some of the observed changes seem to be correlated with ontogeny (growth of gulars, extragulars, caudals, and marginals, disappearance of middorsal keel on the carapace). Several specimens show abnormal layout of scute sulci, several others unusual morphologies of vertebral scute areas, one has an additional pair of plastral scutes, and one extraordinarily pronounced, likely pathological, growth rings on the carapace. Both species are represented in a wide spectrum of sizes, from hatchlings to old, mature individuals. The largest fragmentary specimens of *P. porebensis* allow estimation of its maximal carapace length at approximately 80 cm, while *P. robusta* appears to have reached lower maximal sizes.

Discussion. This is the second contribution describing variability among numerous specimens of Triassic turtles, and the first to show evidence of unambiguous shell abnormalities. Presented data supplement the sparse knowledge of shell scute development in the earliest turtles and suggest that at least some aspects of the developmental programs governing scute development were already similar in the Late Triassic to these of modern forms.

1 Shell variability in the stem turtles *Proterochersis* spp.

2 Tomasz Szczygielski[1,2], Justyna Słowiak[1], Dawid Dróżdż[1]

3 [1] Department of Evolutionary Paleobiology, Institute of Paleobiology, Polish Academy of
4 Sciences, Warsaw, Poland

5 [2] Department of Paleobiology and Evolution, Faculty of Biology, Biological and Chemical
6 Research Centre, University of Warsaw, Warsaw, Poland

8 Corresponding Author:

9 Tomasz Szczygielski

11 Email address: t.szczygielski@twarda.pan.pl

12 **Abstract**

13 **Background.** Turtle shells tend to exhibit frequent and substantial variability, both in bone and

14 scute layout. Aside from secondary changes, caused by diseases, parasites, and trauma, this

15 variability appears to be inherent and result from stochastic or externally-induced flaws of

16 developmental programs. It is, thus, expected to be present in fossil turtle species at least as

17 prominently, as in modern populations. Descriptions of variability and ontogeny are, however,

18 rare for fossil turtles, mainly due to rarity, incompleteness, damage, and post-mortem

19 deformation of their remains. This paper is an attempt at description and interpretation of

20 external shell variability in representatives of the oldest true turtles, *Proterochersis robusta* and

21 *P. porebensis* (Proterochersidae, the sister group to all other known testudinatans) from the Late

22 Triassic (Norian) of Germany and Poland.

23 **Methods.** All the available shell remains of *Proterochersis robusta* (13 specimens) and *P.*

24 *porebensis* (275 specimens) were studied morphologically in order to identify any ontogenetic

25 changes, intraspecific variability, sexual dimorphism, and shell abnormalities. To test the

26 inferred sexual dimorphism, shape analyses were performed for two regions (gular and anal) of

27 the plastron.

28 **Results.** *Proterochersis* spp. exhibits large shell variability, and at least some of the observed

29 changes seem to be correlated with ontogeny (growth of gulars, extragulars, caudals, and

30 marginals, disappearance of middorsal keel on the carapace). Several specimens show abnormal

31 layout of scute sulci, several others unusual morphologies of vertebral scute areas, one has an

32 additional pair of plastral scutes, and one extraordinarily pronounced, likely pathological, growth

33 rings on the carapace. Both species are represented in a wide spectrum of sizes, from hatchlings

34 to old, mature individuals. The largest fragmentary specimens of *P. porebensis* allow estimation

35 of its maximal carapace length at approximately 80 cm, while *P. robusta* appears to have reached

36 lower maximal sizes.

37 **Discussion.** This is the second contribution describing variability among numerous specimens of

38 Triassic turtles, and the first to show evidence of unambiguous shell abnormalities. Presented

39 data supplement the sparse knowledge of shell scute development in the earliest turtles and

40   suggest that at least some aspects of the developmental programs governing scute development

41   were already similar in the Late Triassic to these of modern forms.

Introduction

44   The shell of turtles, although relatively conserved structurally among taxa, tends to show

45   considerable variation between individuals (Parker, 1901; Gadow, 1905; Newman, 1906a;

46   Coker, 1910; Lynn, 1937; Młynarski, 1956; Zangerl & Johnson, 1957; Zangerl, 1969; McEwan,

47   1982; Rothschild, Schultze & Pellegrini, 2013; Cherepanov, 2015, 2016; Farke & Distler, 2015;

48   and many others). This variation may be potentially caused by numerous factors, out of which a

49   suboptimal humidity (Lynn & Ullrich, 1950) or temperature (Yntema, 1970) during incubation,

50   and a low genetic variation (bottleneck) within populations (Velo-Antón, Becker & Cordero-

51   Rivera, 2011; McKnight & Ligon, 2014) were proposed. Expressions of atavistic morphologies

52   were frequently cited as a cause of abnormal shell variants (Gadow, 1905; Newman, 1906b;

53   Grant, 1936a,b), but this always remained rather speculative (e.g., Coker, 1905, 1910;

54   Cherepanov, 1989, 2006, 2014) and in most cases it is easy to refute by comparison with the

55   shell composition (number and layout of shell elements) of stem turtles (e.g., Gaffney, 1990; Li

56   et al., 2008; Szczygielski & Sulej, 2016, 2019). In some cases, abnormal morphologies are

57   attained during postnatal life as a result of diseases, parasites, or trauma (Rothschild, Schultze &

58   Pellegrini, 2013, and references therein).

59   Shell variation affects both the bones and scutes of the plastron and carapace, and the frequency

60   of changes within each of these domains varies between the species (e.g., Coker, 1910; Lynn,

61   1937; Zangerl & Johnson, 1957; Zangerl, 1969; McEwan, 1982) and may even differ between

62   sexes within one species (Coker, 1910). Among modern turtles, Cheloniidae are known to have

63   especially variable shells (Kordikova, 2002; Özdemir & Türkozan, 2006; Pritchard, 2008),

64   although large (yet not documented in the literature) variability may also be observed in some

65   pleurodires (Ferreira, pers. comm. 2018). This unequal susceptibility of various turtles, even

66   those inhabiting similar environments, suggests the presence of some control or repair

67   mechanisms that limit appearance of abnormal morphologies with varying efficiency in different

68   taxa or sexes, but the exact molecular or morphogenetic background of these mechanisms is little

69   known. The developmental rules governing the appearance of supernumerary or asymmetric
70   scutes, however, are well explained by recent studies (Cherepanov, 1989, 2006, 2014, 2015;
71   Moustakas-Verho et al., 2014; Moustakas-Verho & Cherepanov, 2015; Moustakas-Verho,
72   Cebra-Thomas & Gilbert, 2017). According to those studies, shell scutes originate from
73   placodes, which develop in strict correlation with body segmentation: lack of placodes, their
74   asymmetry, improper fusion, or appearance of additional placodes on the level of vacant
75   myosepta lead to abnormal (usually asymmetrical) development of scutes. Some scutes (usually
76   cervical and vertebrals) develop from fusion of initially separate, paired placodes. Some
77   developmental information may, therefore, be obtained from the layout of scutes relative to each
78   other (e.g., see Szczygielski, 2017, for discussion on scutation of Triassic turtles) and even from
79   some scute abnormalities. Understanding of scute development is crucial, because shell scutes
80   precede shell bones in development and thus have a large impact on, the external morphology
81   and even layout of the shell bones (e.g., Zangerl, 1939, 1969; Cherepanov, 1989, 2006, 2016).

82   Various congenital changes to the typical shell structure differ in severity. Cherepanov (2016)
83   classified them into three main categories: malformations (severe developmental flaws, usually
84   lethal or severely detrimental), anomalies (changes to the number and layout of shell elements,
85   not severely detrimental, possibly adaptive), and individual variation (minor changes to the
86   number and layout of shell elements, neutral to normal function). Based on this classification,
87   anomalies and individual variations are much more common than malformations and, out of the
88   former two, anomalies are generally easier to spot and understand in the fossil record, because
89   they are usually more pronounced, frequently asymmetrical, and easier to differentiate from post-
90   mortem deformation.

91   Turtle shells preserve relatively easily in the fossil record, but still, many extinct turtle taxa are
92   known from relatively few, incomplete and/or distorted specimens. For that reason, descriptions
93   of their variability and ontogeny are rare, especially for Mesozoic forms (Gaffney, 1990; Lichtig
94   & Lucas, 2017; Sullivan & Joyce, 2017). Here, we describe the external variability and
95   abnormalities observed in the carapace and plastron of *Proterochersis robusta* Fraas, 1913 and
96   *P. porebensis* Szczygielski & Sulej, 2016 (Figs 1–10, S1–S8) – representatives of the earliest
97   branch of true (total-group) turtles (Testudinata) (Szczygielski & Sulej, 2016).

98

Materials & Methods

Institutional abbreviations

CSMM. Carl-Schweizer-Museum, Murrhardt, Germany.

SMNS. Staatliches Museum für Naturkunde, Stuttgart, Germany.

ZPAL. Roman Kozłowski Institute of Paleobiology, Polish Academy of Sciences, Warsaw, Poland.

Proterochersis robusta

Proterochersis robusta (Figs 1–3, 6, 8, 9A–C, 10, S5A–C, S6A, S7A–D, S8A–D, Articles S2–S3, and Tables S1–S2) is known from the Late Triassic (middle Norian) Löwenstein Formation, Stuttgart proximities, Germany. For the geological background, see Szczygielski and Sulej (2016) and references therein. All of the existing specimens of that species (SMNS 11396, SMNS 12777, SMNS 16442, SMNS 16603, SMNS 17561, SMNS 17755, SMNS 17755a, SMNS 17756, SMNS 17930, SMNS 18440, SMNS 50917, SMNS 51441, SMNS 56606, SMNS 81917; CSMM uncat.) were studied with exception of SMNS 50918 (an internal mold of the shell). For the detailed description of these specimens see Article S1 and for the chart of scute areas preserved on each of them see Tables S1–S2.

Proterochersis porebensis

Proterochersis porebensis (Figs 4–5, 7–8, 9D–T, 10, S1, S4, S5D–N, S6B–D, S7E–P′, S8E–F, Articles S2–S3, and Tables S3–S4) is known from the lower part of Patoka Member of Grabowa Formation, Poręba, Poland. For geological and paleoenvironmental background, see Sulej et al. (2012), Niedźwiedzki et al. (2014), Szulc et al. (2015), Zatoń et al. (2015), and Szczygielski and Sulej (2016). All of the existing specimens (ZPAL V.39/1–28, ZPAL V.39/34, ZPAL V.39/48–72, ZPAL V.39/155–300, ZPAL V.39/331–366, ZPAL V.39/370, ZPAL V.39/373–404, ZPAL V.39/416–420, and uncatalogued) were studied. For the detailed description of these specimens see Article S1 and for the chart of scute areas preserved on each of them see Tables S3–S4.

125 **Methods**

126 The macrophotographs of the smallest specimens, ZPAL V.39/381 and ZPAL V.39/384, were

127 taken using Keyence Digital Microscope VHX-900F. The terminology used for the shell

128 elements (Fig. 1) follows Zangerl (1969) with the amendment by Hutchison and Bramble (1981).

129 To avoid confusion, we use terms "external" rather than "dorsal", "lateral", or (in case of

130 plastron) "ventral" to describe the scute-covered surfaces of the shell, and "dorsomedial" rather

131 than "dorsal" or "medial" when referring to the parts of the carapacial scute areas located closest

132 to the neural row (at the midline and at the very top of the carapace), with the exception of the

133 cervical and the vertebrals, for which the term "medial" is uncontroversial, and the bridge

134 marginals in ventral aspect, for which "ventromedial" is used to indicate the direction towards

135 the middle point of plastron. Also for clarity, for marginal scutes we use "length" for the

136 dimension of marginal scutes measured radially from the middle to the periphery of the carapace,

137 and "width" for the dimension measured along the edge of the carapace, regardless of the

138 position of the scute and thus its orientation relative to craniocaudal axis of the whole carapace.

139 The edge of the marginal scute contacting scutes other than the preceding or succeeding marginal

140 is called "base", while its free edge is called "rim".

141 **Data acquisition and preparation.** The shape analysis was performed for the gular and anal

142 regions of the plastron. The sample of gular regions includes ten specimens of *Proterochersis*

143 *porebensis* (ZPAL V.39/34, ZPAL V.39/48, ZPAL V.39/49, ZPAL V.39/187, ZPAL V.39/333,

144 ZPAL V.39/379, ZPAL V.39/385, ZPAL V.39/387, ZPAL V.39/388, and ZPAL V.39/420) and

145 one *P. robusta* individual (SMNS 17561). We took photographs of articulated and most

146 complete cranial tips of plastra (areas of gular and extragular scutes) in ventral view.

147 Additionally the shape of the extragulars of *P. porebensis* was analyzed based on the vertical

148 sections of their 3D models. Models were generated photogrammetrically using the freeware

149 program Visual SFM 0.5.26 and the free software MeshLab 2016 (Cignoni et al., 2008; Wu,

150 2011) for the specimens ZPAL V.39/48, ZPAL V.39/187, ZPAL V.39/333, ZPAL V.39/379,

151 ZPAL V.39/385, ZPAL V.39/387, ZPAL V.39/388, and ZPAL V.39/420 and Agisoft Photoscan

152 1.2.0 (www.agisoft.com) for ZPAL V.39/34 and ZPAL V.39/49. In the case of the *P. robusta*

153 specimen SMNS 17561 (the only specimen of that species fully preserving that region) the 3D

154 modeling was impossible to perform because the specimen is not sufficiently prepared and the

155 extragulars are only exposed ventrally. To create the models with Visual SFM and MeshLAB,
156 around 100 photos from angles of 0º, 15º, and 40º were taken. To speed up the process of the
157 model generation, the photographs were scaled down to resolution 800x600 px by the freeware
158 program FastStone Photo Resizer 3.8 (www.faststone.org) with the exception of ZPAL
159 V.39/385, for which photographs of resolution 6000x4000 px were used. For the specimens
160 ZPAL V.39/34 and ZPAL V.39/49, around 200 of 6000x4000 px photos were used to obtain
161 models of whole shells, and then the cranial plastral sections were separated using MeshLab.
162 Model of each specimen was then scaled in MeshLab to match its original size and the
163 extragulars were digitally sectioned in sagittal plane. For sectioning the best preserved
164 extragulars were chosen: right extragulars of ZPAL V.39/49, ZPAL V.39/187, ZPAL V.39/333,
165 ZPAL V.39/379, ZPAL V.39/388, left extragulars of ZPAL V. 39/34, ZPAL V.39/387, ZPAL
166 V.39/420 right and left extragulars of ZPAL V.39/48 and ZPAL V.39/387. The 3D models used
167 for the analysis are shown in the online appendices Articles S2–S3.

168 For the anal region, we took photographs of the best preserved caudal tips of plastra (caudal
169 processes and intercaudal scute) in ventral view. We analyzed seven *P. porebensis* (ZPAL
170 V.39/34, ZPAL V.39/48, ZPAL V.39/49, ZPAL V.39/66, ZPAL V.39/69, ZPAL V.39/70, and
171 ZPAL V.39/71) and three *P. robusta* individuals (CSMM uncat., SMNS 12777, and SMNS
172 17561). The photographs were converted to the .TPS format using the tpsUtil 1.76 program
173 (Rohlf, 2015).

174 A set of five landmarks on the gular region in ventral view, two in the vertical section of the
175 extragulars, and another five on the anal region were digitalized using the software tpsDig 2.31
176 (Rohlf, 2015). All landmarks are of Bookstein's (1997) first type, they point the intersections
177 between element boundaries – herein, the landmarks mark intersections between the sulci (see
178 Table 1). In order to analyze the shape of curves, we used eight semilandmarks along the cranial
179 curve of the gular and extragular, thirteen along the curve of cross-sectioned extragular, and
180 twelve semilandmarks along the edge of caudal process. The semilandmarks were also taken
181 using tpsDig. In case of minor incompleteness of the element, several semilandmarks were
182 estimated, using the opposite side whenever possible. In four cases (SMNS 17561, ZPAL
183 V.39/49, ZPAL V.39/69, ZPAL V.39/385), complete data from opposite sides of a single
184 individual were averaged. The gular and the anal regions were digitized twice.

185   **Geometric morphometric analyses.** All geometric morphometric analyses were performed in

186   MorphoJ 1.06d (Klingenberg, 2009, 2011). First, generalized Procrustes analysis (GPA) was

187   performed to remove the information related to size, position, and orientation (Zelditch et al.,

188   2004). Then, we averaged the shape data for left and right sides for ZPAL V.39/49, ZPAL

189   V.39/69 and ZPAL V.39/385. Wireframe graphs and Principal Component Analyses (PCA) were

190   used to visualize shape differences of gulars, extragulars, and caudal processes. Significance of

191   the differences in shape between the groups identified form the PCA plots were assessed using

192   the Procrustes Analysis of Variance (ANOVA), analogous to MANOVA (Klingenberg, 2009,

193   2011). A multivariate regression of the caudal processes and gular shape against log-transformed

194   centroid size on pooled within-group (by species) variation was conducted for the presence of

195   allometries (Klingenberg, 1996).

196   The Pearson product-moment correlation coefficients used for simple estimations of the shell

197   sizes of exceptionally large, fragmentary specimens were calculated in Microsoft Office

198   Standard 2010 Excel (v. 14.0.7212.5000, 64-bit) using the CORREL function. These calculations

199   are based on very small sample sizes, therefore they should be understood as auxiliary only.

200

201   **Results**

202   **Specimen sizes.** Shell material of *Proterochersis robusta* consists of thirteen specimens of

203   varying sizes and, supposedly (inferred on size and morphology), ontogenetic age spanning from

204   a young, not yet fully ossified juvenile (SMNS 81917, Fig. S6A) to large, apparently mature,

205   individuals (e.g., SMNS 16442, Figs 2C, 3D, or SMNS 18440, Figs 2K, 3H). Shell remains of *P.*

206   *porebensis* are much more numerous (270 catalogued specimens), but usually much more

207   fragmentary, frequently consisting of parts of costals, small sections of plastron or the rim of the

208   shell, or other uninformative elements, and only four relatively complete shells (ZPAL V.39/34,

209   ZPAL V.39/48, ZPAL V.39/49, and ZPAL V.39/72) were found thus far (Figs 4–5).

210   Similarly to *P. robusta*, the collected specimens of *P. porebensis* represent a wide spectrum of

211   sizes and morphologies, probably representing various ontogenetic ages. The smallest known

212   individual appears to be a hatchling or a very young juvenile, and is represented by an

213   exceptionally small, fragmentary costal (ZPAL V.39/381, Fig. S1C–D). ZPAL V.39/34 (Figs

214   4A–B, 5A, 9K, S4C, S5G, S7E–G) is more developed and much larger (approx. 28 cm of

215   carapace length; note that shell lengths are approximate due to damage and distortion), but still

216   differs morphologically from the larger specimen and thus may be tentatively classified as an

217   older juvenile. ZPAL V.39/48 (Figs 4C–D, 5B, 9G, S2A–B, S5H, S7H–J) is even larger (approx.

218   42.5 cm of carapace length) and exhibits shell morphology typical for large individuals but is

219   tentatively classified as a subadult based on incompletely ossified dorsal process of the scapula

220   (following Gaffney, 1990; see Szczygielski & Sulej, 2016). ZPAL V.39/72 (Figs 4G–H, S4D,

221   S5K) is of comparable size (approx. 44.5 cm of carapace length) and seems to be of comparable

222   ontogenetic age. ZPAL V.39/49 (Figs 4E–F, 5C, 9D, S2C–F, S5I, S7K–M) is the largest

223   complete shell found thus far (approx. 49 cm of carapace length) and thus is treated as an adult,

224   but some fragmentary specimens, such as ZPAL V.39/8 (see Szczygielski & Sulej, 2019), ZPAL

225   V.39/57 (Figs S1N, S3B), ZPAL V.39/60 (Fig. S1O–P), and ZPAL V.39/63 (Fig. S1A–B)

226   indicate that this species could have reach even larger sizes. ZPAL V.39/63 (a carapace fragment

227   with dorsal part of ilium attached) seems to be particularly large – around the contact with the

228   ilium, the carapace is up to 1.5 cm thick, the sulci are very wide (see below), and the ilium is

229   massive, being at the point of attachment to the carapace 6.3 cm broad (measured from the lateral

230   edge of the bulge to the base of the first sacral rib), compared to 3.5 cm in ZPAL V.39/48, 4 cm

231   in ZPAL V.39/49, and 3.7 cm in ZPAL V.39/72. Accurate measurement of ilium breadth is

232   difficult in ZPAL V.39/34 due to damage and surrounding rock matrix, but it seems to be about 2

233   cm. Based on these data, it seems that there is a strong correlation between the breadth of the

234   dorsalmost end of the ilium and the length of the carapace (Pearson correlation coefficient =

235   0.997 with ZPAL V.39/34 included and 0.995 with that specimen excluded; n = 4 or n = 3,

236   respectively), although the small number of specimens must be taken into account. Based on

237   that, the carapace length of ZPAL V.39/63 may be estimated to be between 75 and 80 cm

238   (depending on whether the measurement of ZPAL V.39/34 is considered). With the exception of

239   ZPAL V.39/34, the collected complete shells of *P. porebensis* are larger than all known shells of

240   *P. robusta* (possibly excluding the fragmentary specimens SMNS 16442 and SMNS 18440, as

241   their exact size is difficult to estimate).

242   It must be kept in mind that in most cases it is very difficult or outright impossible to accurately

243   estimate the ontogenetic age or even general ontogenetic stage of fossil animals, especially when

244   the specimens are fragmentary and no skeletochronological data are at hand. Usually, the only

245   readily available proxy for the relative age of the individuals is their size and, in some cases,

246   advancement of the skeletogenesis (ossification of the articular surfaces of long bones, closure of

247   fontanelles, fusion of sutures, etc.). The sizes and tempo of ossification in the animals of the

248   same age may, however, differ within the population depending, e.g., on their sex or

249   environmental conditions (e.g., Berry & Shine, 1980; Pritchard, 2008; Farke & Distler, 2015).

250   For that reason, animals of different sizes may be of comparable ontogenetic age and animals of

251   similar size may in fact represent different age groups. Based on some consistent combinations

252   of size and morphological characteristics, in the studied material of *Proterochersis* spp. several

253   ontogenetic stages may be provisionally recognized – most notably supposed juveniles (small,

254   sometimes not fully ossified shells, weakly developed gular and extragular tubercles and caudal

255   processes, straight margins of the shell, etc.), adults (medium-sized shells, prominent gular and

256   extragular tubercles, well-developed caudal processes and features of the shell margin, etc.), and

257   old individuals (largest shells, most pronounced superficial characteristics of the shell; see below

258   for detailed characterization). For convenience, these categories will be evoked in the

259   descriptions, but they are of course tentative, given the aforementioned problems, and not

260   entirely discrete. For now, they should be treated as generalized morphotypes with implied

261   ontogenetic meaning. Obviously, it is unknown at which point these animals attained sexual

262   maturity, so our classification into the juveniles and adults is based solely on morphological

263   terms, although it seems possible that at least some of the adult-like characters (particularly the

264   pronounced gulars, extragulars, and caudals) may be related to sexual selection or copulation.

265   Skeletochronology will probably be attempted for *P. porebensis* in the future and these

266   categories will possibly be validated.

267   There is some incongruency between these large maximal sizes and the moment of shell

268   ankylosis. Typically, the ankylosis stops the growth of the shell, because the bones grow mainly

269   along the sutures (Pritchard, 2008). Most specimens of *Proterochersis* spp., however, are fully

270   ankylosed, regardless of their size. Even if the prevalence of ankylosed specimens in Poręba and

271   localities around Stuttgart may be a preservation or sorting artifact (e.g., the unankylosed

272   specimens were typically destroyed by currents or small fragments of disarticulated unankylosed

273   shells were buried elsewhere; see Szczygielski & Sulej, 2019), the fact that ankylosis occurred

274   even in relatively small specimens with juvenile features (e.g., ZPAL V.39/2, ZPAL V.39/34,

275   ZPAL V.39/66) is more troubling. Many of these small specimens are well-preserved and it is

276   hard to imagine that the sutures were obliterated by some diagenetic processes, while minor

277   details of shell anatomy and texture remained intact. In some turtle species the sexual

278   dimorphism takes form of a striking difference of sizes between mature males and females

279   (Pritchard, 2008). In such a case, specimens like ZPAL V.39/34 could be considered one of the

280   sexes, and large specimens like ZPAL V.39/49 – the other one. This, however, seems to be

281   refuted by a fact that there exists a full spectrum of sizes of ankylosed specimens between ZPAL

282   V.39/34 and ZPAL V.39/49 (e.g., ZPAL V.39/48 with subadult characters). Likewise, this would

283   preclude interpretation of small ankylosed specimens as a separate species. In lack of other likely

284   explanations, a very broad variation in time of ankylosis is therefore provisionally accepted.

285   Another possible solution is seasonal hypercalcifiaction and decalcification of sutures or shell

286   bones that could increase the rigidness of the shell mosaic (see Szczygielski & Sulej, 2019) but

287   also allow seasonal growth – similar mechanism of de-ossification was reported locally in the

288   mid-section of plastron in males of some modern turtles during mating season (Wibbels, Owens

289   & Rostal, 1991; Wyneken, 2001; Pritchard, 2008). Finally, the growth might have occurred

290   mainly by the means of bone remodeling. This problem may be resolved by future histological

291   studies.

292   With very few exceptions, the specimens of *Proterochersis* spp. are incomplete, and often the

293   overlap between them is small, which makes comparisons or even reliable estimation of their

294   size difficult – even more so, relative proportions of epidermal elements or breadth of plastral

295   lobes may vary between individuals and sometimes even bilaterally within one individual, as

296   evidenced by several relatively complete shells. For that reason, it is impossible to confidently

297   estimate the shell length based on, e.g., the length of a single plastral scute. These differences in

298   proportions are difficult to explain, and incompleteness or poor preservation of the specimens

299   makes it currently impossible to determine if they result, e.g., from allometric growth, sexual

300   dimorphism, or are just part of normal intraspecific variability.

301   See Table S5 for the collection of most important measurements of *Proterochersis* spp. given in

302   the text.

303   **Carapace**

Costals. ZPAL V.39/381 (Fig. S1C–D) is a fragmentary costal of the smallest, and probably the youngest, known individual of *Proterochersis porebensis*. This costal is 8 mm wide, 2 mm thick in the peripheral regions, and 3 mm thick at the ventral ridge. It appears to lack natural edges with exception of a portion of proximal (medial) rim. The gracility of that element, its smooth external surface with subtle longitudinal striation, lack of the typical rough texture indicative of contact with superficial layers of dermis, and a rounded convexity in the proximal region of the external surface (Fig. S1C) suggest, however, that it is not a part of a full-sized costal.

The widest costal with preserved sutural edges is ZPAL V.39/176 (5.1 cm wide, 5 mm–1.2 cm thick, Fig. S1E). Its width suggests that it comes from an individual similar in size to ZPAL V.39/49. The structure of the sutures is relatively simple (longitudinally lamellar) in that specimen and the thickness is intermediate, compared to some other specimens (see Szczygielski & Sulej, 2019), even if they are narrower. This probably results from the position of the costal within the shell – as a general rule, the posterior costals seem to be narrower in *Proterochersis* spp. than the anterior ones. Thus, it is likely that the thicker costals with more developed sutural edges, such as ZPAL V.39/3 (see Szczygielski & Sulej, 2019) come from ontogenetically older specimens, but from more caudal part of the shell.

Vertebrae. ZPAL V.39/377 (Figs S1H–K, S2I) is a fragment of the dorsal section of the vertebral column of a young *Proterochersis porebensis* individual, consisting of one and a half vertebra. Besides the relatively small size (the complete vertebra is 1.9 cm long, 1.2 cm wide at the level of facets for the ribs), it differs from all other known vertebrae of *Proterochersis* spp. in lack of ankylosis and neurals. The natural bone limits are visible, proving that the dorsal ribs in proterochersids were already shifted cranially to an intervertebral position typical for turtles. The facets for the ribs (Fig. S1I) are ovoid, longer than high, higher caudally than cranially, gently skewed cranioventrally in lateral view, and at least in ¾ of their length they are located in the cranial part of the centrum. Likewise, the neural spines are also inclined slightly cranially. The neurocentral sutures cross the articulation facets for ribs, their inclination is slightly oblique, dorsocaudal, and generally agrees with the inclination of the facets. The zygapophyses are small and roughly triangular. The centra are hourglass-shaped in ventral view (Fig. S1J). Along the long axis of the centra, their ventral surfaces are gently projected ventrally. As they are preserved, the vertebrae are separated by a gap approx. 3 mm wide (Fig. S1I, J), probably filled

334   in life by the intervertebral disc or unossified, cartilaginous ends of the centra. The neural canal,

335   exposed caudally, is very high and narrow, measuring up to 8 mm in height and 2.5 mm in width

336   (Fig. S1H). The most surprising is the dorsal surface of the neural spines (Fig. S1K). Neurals are

337   absent, but there is no sign of bone breaking, and no cancellous bone is exposed. Instead, the

338   surface is bumpy and perforated by numerous vascular canals. This does not resemble a suture;

339   there are no lamellae nor spikes. For that reason, we interpret this either as a sign of a

340   cartilaginous cap on the dorsal ends of neural spikes (albeit it is located relatively high and the

341   neural spikes are broadened dorsally, Fig. S1H) or as incipient intramembranous ossification,

342   just beginning the development of neurals. In either case, it indicates young ontogenetic age of

343   the individual.

344   All the other specimens of *Proterochersis* spp. that preserve dorsal vertebrae, including SMNS

345   56606, ZPAL V.39/48 (see Szczygielski & Sulej, 2016; Szczygielski, 2017), ZPAL V/39/49 (see

346   Szczygielski, 2017), ZPAL V.39/72 (see Szczygielski & Sulej, 2016; Szczygielski, 2017), ZPAL

347   V.39/169 (Figs S2G, S4E–F, comparable in size with ZPAL V.39/49), and ZPAL V.39/378 (Figs

348   S1F–G, S2J comparable in size with ZPAL V.39/49) have their dorsal vertebral columns fully

349   ankylosed, and no unambiguous intervertebral and costovertebral articulation points or sutures

350   can be seen. In these larger (and supposedly ontogenetically older) specimens the dorsal

351   vertebrae get obviously larger and more robust, particularly at the points of articulation. The

352   ventral surfaces of the dorsal vertebrae of ZPAL V.39/48 (with exception of the first and the last

353   three dorsal vertebra) form a relatively sharp midventral ridge (Fig. S2B; see Szczygielski &

354   Sulej, 2016), and a sharpened ridge can be seen on the mid-dorsal vertebra of ZPAL V.39/49

355   (Fig. S2C–D), but in the remaining specimens the ventral surface is more rounded. Given the

356   limited sample, it is difficult to tell if this is related to ontogeny or just variable in the population.

357   It seems that this sharpened ridge is more frequent in the mid-section of the dorsum than in the

358   cranial or caudal end of the dorsal vertebral column (Fig. S2). The dorsal neural canal of ZPAL

359   V.39/49 (Fig. S2C, S2E), ZPAL V.39/169 (Fig. S2G), ZPAL V.39/378 (Fig. S2J), and ZPAL

360   V.39/402 (Fig. S2K), as exposed, is closer to circular in cross-section and measures approx. 4

361   mm x 5 mm in ZPAL V.39/169 and ZPAL V.39/378, approx. 8 mm x 7 mm in ZPAL V.39/49,

362   and approx. 8 mm x 1 cm in ZPAL V.39/402. The cranial opening of the dorsal canal at the

363   cranial end of the first dorsal vertebra in ZPAL V.39/48 is more subtriangular or ovoid and

364   measures approx. 7 mm x 6 mm (Fig. S2A). The observations made during the preparation of

365   ZPAL V.39/49 indicate that the shape of the canal changes craniocaudally (more oval in the parts

366   with the sharp ventral ridge, more circular caudally; no exact measurement were taken at the

367   time; Fig. S2C-F), but never seem to approach the proportions seen in ZPAL V.39/377.

368   Similarly, the cross-section of the mid-dorsal vertebral column exposed during preparation in

369   ZPAL V.39/48 (Fig. S2B) reveals a circular neural canal (also not measured, but the width to

370   height ratio approached 1:1). ZPAL V.39/370 shows a circular neural canal (8 mm x 7 mm) in

371   the cross-section of the first sacral vertebra (Fig. S2H) and ZPAL V.39/402 shows a triangular

372   neural canal (1 cm x 9 mm) the end of the second sacral vertebra (both co-ossified with the

373   carapace; Fig. S2L). Although compaction might have potentially had some impact on the shape

374   of the vertebral canal in mentioned specimens, no significant deformation is apparent.

375   **Cervical scute.** In adult and subadult individuals of *Proterochersis robusta* and *P. porebensis*

376   the cervical was trapezoidal to crescent-shaped (Figs 1–2, 4, 6B–C, S1N, S3). The caudal (basal)

377   edge, contacting the cranialedge of the first vertebral scute, was longer than the cranial. The

378   shortest, slanted, craniolateral edges contacted the mediocaudal edges of the first pair of

379   marginal scutes. The lateral tip of the cervical scute may form a several millimeter long contact

380   with the base of the second marginal scute (e.g., *P. porebensis* specimens ZPAL V.39/57, Figs

381   S1N, S3B, and ZPAL V.39/49, Fig. 4E), merely touch the second marginal (e.g., *P. porebensis*

382   ZPAL V.39/48, Fig. 4C, and ZPAL V.39/72, Fig. 4G), or such a contact may be prevented by the

383   first marginal (e.g., *P. robusta* SMNS 17561, Fig. 2F, and SMNS 17930, Figs 2I, 6B–C; *P.*

384   *porebensis* ZPAL V.39/22, Fig. S3A) – these morphologies seem to not be discrete, but rather

385   form a continuous series of variable relative positions of the lateral tip of the cervical and the

386   sulcus between the first two marginals. In *P. porebensis* specimen ZPAL V.39/34 (Fig. 4A) the

387   cervical was more rectangular, with roughly craniocaudally directed lateral edges. In ZPAL

388   V.39/34 (Fig. 4A) the cervical is 8 mm long, in ZPAL V.39/390 (Fig. S1L) it is 1 cm long, in

389   ZPAL V.39/22 (Fig. S3A) and ZPAL V.39/48 (Fig. 4C) it measures 1.5 cm in length, in ZPAL

390   V.39/72 (Fig. 4G) it is 1.9 cm long, and in ZPAL V.39/49 (Fig. 4E) it is 2.2 cm long. ZPAL

391   V.39/57 (Fig. S1N) has the longest cervical, measuring 2.4 cm. In most specimens the cervical

392   scute breadth did not exceed 1/3 of the width of the first vertebral scute, but in ZPAL V.39/49

393   the cervical is wider than a half of the first vertebral (Fig. 4E). It remains uncertain whether this

394   is correlated with the presence of paired nuchal bone (see Szczygielski & Sulej, 2019) or if it

395   results, e.g., from allometry.

Vertebral scutes. *Proterochersis* spp. had a single row of five broad vertebral scutes, which
covered most of the dorsal surface of the carapace (Figs 1–2, 4, 6). The first vertebral was fan-
shaped, with a rounded medial process directed caudally, which was received by an cranial
medial notch of the second vertebral. AnterThe cranial edge was gently bowed, it contacted the
caudal (basal) edge of the cervical, the base of the second marginal, and (usually) cranial portion
of the base of the third marginal (*P. porebensis* ZPAL V.39/57, Figs S1N, S3B, being the only
known exception due to the second marginal preventing such contact). In some specimens (e.g.,
P. robusta specimens SMNS 17561, Fig. 2F, and SMNS 17930, Figs 2I, 6B–C, and *P.
porebensis* ZPAL V.39/22, Fig. S3A) there is a minor contact between the first vertebral and the
caudal portion of the base of the first marginal scute. Laterally, the first vertebral formed facets
for contact with the first pair of pleurals. The length of these facets proportionally to the scute
area increased with the size of the animal, in large individuals (such as *P. porebensis* ZPAL
V.39/49, Fig. 4E, and ZPAL V.39/57, Fig. S1N) reaching over 3.5 cm. The first vertebral in
some specimens was slightly asymmetrical – in SMNS 17561 its left caudolateral margin was
more concave than the right one (Fig. 2F), in ZPAL V.39/49 the scute was expanded slightly
more to the right than to the left (Fig. 4E), and in ZPAL V.39/72 the caudalmost point of the
caudal process seems to be shifted to the left relative to the midline (Figs 4G). These changes do
not seem to result from the crushing or compaction of the specimens.

The cranial edge of the second vertebral was bow-shaped, with a rounded medial embayment
which received the caudal process of the first vertebral scute. Craniolaterally, it contacted the
dorsomedial edges of the first pair of pleurals, laterally it contacted about 3/5 of the dorsomedial
edge of the second pair of pleurals, and caudally it contacted the cranial edge of the third
vertebral scute. The second vertebral is widest in its caudal part, at (or slightly caudal to) the
level of the sulcus between the first and the second pleural. The remaining vertebrals were
roughly trapezoidal, each scute slightly narrower caudally than cranially, and had generally
straight cranial edges. The third vertebral contacted the second vertebral cranially, the remaining
part of the dorsomedial edge of the second pair of pleurals and over 2/3 of the dorsomedial edge
of the third pair of pleurals laterally, and the fourth vertebral scute caudally. It was widest around
the sulcus between the respective pleurals, and in dorsal view its width was comparable to the
width of the second vertebral (although it might have been slightly larger measured along the
surface due to shell curvature – this, however, in most specimens is obscured by deformation or

427 breakage). The fourth vertebral contacted the third cranially, the remaining part of the

428 dorsomedial edge of the third pair of pleurals and the whole dorsomedial edge of the fourth pair

429 of pleurals laterally, and the fifth vertebral scute caudally. The widest point of that scute lied in

430 its cranial part. The fifth vertebral was more semi-dome-shaped than the vertebrals first to fourth.

431 It contacted the preceding vertebral cranially and the caudal edges of the last (fourth) pair of

432 pleurals craniolaterally. Laterally and caudolaterally, it contacted the bases of the caudalmost

433 marginals – usually the 12th, the 13th, and the 14th, although sometimes there was no contact with

434 the 12th and at least in ZPAL V.39/48 the 15th pair of marginals was present (see below).

435 Caudally, in *Proterochersis* spp. there was a caudal notch (Fig. S3). The variability in the

436 vertebral scutes 2–5 is mostly evident medially.

437 In two small specimens of *Proterochersis porebensis* (ZPAL V.39/2, Fig. S4A–B; ZPAL

438 V.39/34, Figs 4C, S4C, see Sulej, Niedźwiedzki & Bronowicz, 2012; Szczygielski & Sulej,

439 2016) a pronounced medial ridge is present crossing the area of the second, the third, and the

440 fourth (in ZPAL V.39/34; in ZPAL V.39/2 this part is missing) vertebral scute. The ridge is

441 rounded to triangular in cross-section, laterally symmetrical, and for most of its length

442 surrounded laterally by deep troughs. Cranially, the ridge and the troughs gradually even out,

443 they tend to nearly disappear in the caudalmost parts of the vertebral scute areas, just before the

444 intervertebral sulci, and in ZPAL V.39/34 the ridge disappears caudally before the throughs do,

445 resulting in a shallow, longitudinal, midline depression in the caudal part of the fourth vertebral

446 scute area (Fig. S4C). The external morphology and small distance between the ribs in ZPAL

447 V.39/2 indicate that it was similar in size to ZPAL V.39/34, which suggests that this morphology

448 of the middorsal keel is related to the young ontogenetic age of the individuals. In *P. porebensis*

449 specimens ZPAL V.39/1 (Fig. S4G–H), ZPAL V.39/4 (see Szczygielski & Sulej, 2019), ZPAL

450 V.39/72 (Fig. S4D), and ZPAL V.39/169 (Fig. S4E–F), and on a small midcarapacial fragment

451 of *P. robusta* specimen SMNS 11396, a much more subtle, low, and rounded midline ridge can

452 be seen with equally subtle lateral troughs or no troughs at all. If the middorsal keel of ZPAL

453 V.39/2 and ZPAL V.39/34 is interpreted as a juvenile character, then it seems probable that the

454 middorsal ridges of larger SMNS 11396, ZPAL V.39/1, ZPAL V.39/4, and ZPAL V.39/72 may

455 represent remnants of that structure. No midline ridges can be found in ZPAL V.39/48 (slightly

456 smaller than ZPAL V.39/72 and, judging by rib spacing, comparable in size to ZPAL V.39/1) or

457 ZPAL V.39/49, but the carapaces of these two specimens are broken along the midline, possibly

458   obscuring the ridges. The ridge in ZPAL V.39/1 is slightly tilted cranially to the left, so in the

459   cranial part of the specimen it loses strict correlation with underlying neural processes of the

460   vertebrae (Fig. S4G–H). This supports the view that middorsal ridges of proterochersids are not

461   strictly induced by the position of the axial skeleton, but rather are related to epidermal scutes.

462   Three *P. robusta* specimens (CSMM uncat., Fig. 2A; SMNS 17561, Fig. 2F; SMNS 17930, Figs

463   2J, 8) exhibit various degrees of indentation along the midline of the second, the third, and the

464   fourth vertebral scute areas. The most severe case is exhibited by CSMM uncat. (Fig. 2A). Along

465   the midline in the cranial regions of the second and the third vertebral, deep, funnel-shaped

466   grooves are present, as if the scute area was cranially split in two. These grooves are

467   approximately as deep as the cranial vertebral sulci with which they are connected, they

468   penetrate the vertebral fields no further than to the mid-length, and caudally they become

469   noticeably shallower and narrower, ending in a sharpened point. In the caudal parts of the scute

470   areas they continue as subtle depressions. The third vertebral lacks the deep groove, but there is a

471   similarly shaped, shallow depression. The fifth vertebral is depressed as well, but the depression

472   is wider and gentle. In SMNS 17930 (Figs 2I, 6) the anatomy is similar, but less pronounced –

473   there are weak grooves in the cranial parts of the second and the third vertebral area, similar to

474   the caudal sections of the grooves of CSMM uncat., and there is a gentle depression running

475   along the middle of the shell. SMNS 17561 (Fig. 2F) exhibits only a weak depression along the

476   midline, only slightly more pronounced in the cranial sections of the vertebral areas. This

477   morphology initially resembles the midline troughs of ZPAL V.39/2 (Fig. S4A) and ZPAL

478   V.39/34 (Figs 4A, S4C) but there are several important differences. Firstly, in CSMM uncat.,

479   SMNS 17561, and SMNS 17930 there is no middorsal keel. Secondly, these specimens are

480   relatively large (SMNS 17561 is approx. 35 cm long, SMNS 17930 is approx. 36 cm long, and

481   CSMM uncat. is over 36.5 cm long; note that the damage suffered by SMNS 17930 and CSMM

482   uncat. may cause some underestimation of their sizes and/or relative size differences). Thirdly,

483   the middorsal keels and troughs of ZPAL V.39/2 (Fig. S4A) and ZPAL V.39/34 (Figs 4A, S4C)

484   do not reach the cranial edge of the second vertebral and span along the full length of the third

485   vertebral, but do not connect to intervertebral sulci, while the midline grooves or depressions of

486   CSMM uncat. (Fig. 2A), SMNS 17561 (Fig. 2F), and SMNS 17930 (Figs 2I, 6A–C) are most

487   pronounced near the cranial edges of the vertebral scutes and in CSMM uncat. they connect to

488   intervertebral sulci. Considering that the vertebral scutes grew mostly in their cranial part (see

489   below), it seems likely that these depressions and grooves developed relatively late during

490   ontogeny, and may be evidence of scute splitting. Congruent with this hypothesis is the observed

491   positive correspondence between the severity of observed morphologies and the size of the

492   specimens. The presence of that morphology on the vertebral scute areas of *P. robusta* specimen

493   SMNS 16442 (Fig. 2C) is ambiguous. A shallow groove seems to be present medially, but this

494   specimen is compacted, broken, and its surface is poorly preserved, making assessment difficult.

495   In *Proterochersis robusta* specimen SMNS 17930 (Figs 2I, 6) and in several specimens of *P.*

496   *porebensis* (ZPAL V.39/4, see Szczygielski & Sulej, 2019; ZPAL V.39/34, Figs 4A, S4C; ZPAL

497   V.39/49, Fig. 4E; ZPAL V.39/72, Figs 4G, S4D; ZPAL V.39/169, Fig. S4E) the sulci separating

498   the first and the second, the second and the third, and/or the third and the fourth vertebral scute

499   area form in the middle small, arrow-shaped cranial projection. In some cases (ZPAL V.39/4,

500   ZPAL V.39/34, ZPAL V.39/72) this projection is laterally surrounded by two rounded caudal

501   projections, resulting in a ω-shaped pattern. The presence of the cranial projection seems to be

502   correlated with, but not exclusive to, the presence of a middorsal keel or ridge.

503   The intervertebral sulci of most *Proterochersis* spp. specimens, although relatively straight

504   compared to, e.g., circumpleural sulci, exhibit some minor irregularities. In many cases, it is

505   difficult to evaluate whether these irregularities are an effect of post-mortem distortion.

506   Curiously, however, the sulcus between the third and the fourth vertebral seems to be

507   comparatively more prone to severe irregularities. In *P. robusta* specimen CSMM uncat. (Fig.

508   2A) it is clearly asymmetrical in the middle section, where it spans cranially, and an asymmetry

509   of the same sulcus is also profound in another *P. robusta* specimen, SMNS 17561 (Fig. 3F) – in

510   that case the sulcus is wavy rather than straight and skewed, so it meets the third pleural more

511   cranially on the right side than on the left. Similarly to CSMM uncat., the mid-section of this

512   sulcus is asymmetrical in *P. porebensis* specimen ZPAL V.39/34 (Fig. 4A).

513   **Pleural scutes.** *Proterochersis* spp. had paired rows of four polygonal, slightly elongated pleural

514   scutes (Figs 1–2, 4, 6, S5). The first pleural was hexagonal. In all the specimens of

515   *Proterochersis* spp. it contacted the first vertebral mediocranially via dedicated facet, and the

516   relative length of this facet seems to increase with the size of the animal (Figs 2, 4). In this

517   respect, *Proterochersis* spp. differed from *Keuperotersta limendorsa* Szczygielski & Sulej, 2016,

518   in which the sulcus between the first vertebral and the first pleural lies in the same line as the

519   sulcus between the first vertebral and the second marginal, and nearly in the same line as the

520   sulcus between the second vertebral and the first pleural. *K. limendorsa*, however, is currently

521   represented by a single specimen, so it is difficult to estimate if this difference is taxonomic,

522   ontogenetic, or an effect of intraspecific variability. Beside the first vertebral, the first pleural

523   contacted the second vertebral dorsomedially, the second pleural caudally, the caudal part of the

524   base of the second marginal (with the exception of *P. porebensis* specimen ZPAL V.39/57, Figs

525   S1N, S3B), the whole base of the third, and the cranial part of the base of the fourth marginal as

526   well as the cranial part of the dorsomedial edge of the first supramarginal ventrolaterally, and the

527   second pleural scute caudally. The second pleural was heptagonal and had contacts with the first

528   pleural (cranially), all three supramarginals (ventrolaterally), the third pleural (caudally), and the

529   second and the third vertebral scute (dorsomedially). The third pleural usually was hexagonal,

530   contacted the second pleural (cranially), the third supramarginal scute and the ninth and tenth

531   marginal (ventrolaterally), the fourth pleural (caudally), and the third and fourth vertebral scute

532   (dorsomedially). In most individuals the sulcus with the ninth and tenth marginal was roughly

533   continuous and straight, but in *P. porebensis* specimen ZPAL V.39/49 (Fig. 4E–F) the basal

534   edges of these scutes were directed at an angle, resulting in a heptagonal third pleural. Less

535   pronounced, but similar condition can be seen also in *P. robusta* specimen SMNS 17561 (Fig.

536   2G) and *P. porebensis* ZPAL V.39/72 (Fig. 4G–H). The fourth pleural was hexagonal and

537   contacted the third pleural (cranially), the bases of the tenth, 11th, and 12th marginal (in some

538   specimens, such as *P. robusta* SMNS 17561, Figs 2F–G, S5B, and *P. porebensis* ZPAL V.39/48,

539   Figs 4C–D, S5H, the caudalmost tip of the last pleural may also touch the cranial tip of the 13th

540   marginal), and the fourth (dorsomedially) and fifth (caudally) vertebral scute. Usually, the

541   interpleural sulci lack pronounced curvature, but in some specimens (e.g., *P. robusta* SMNS

542   17561, Fig. 2F–G, *P. porebensis* ZPAL V.39/48, Fig. 4C–D, and ZPAL V.39/49, Fig. 4E–F) the

543   caudal edges of pleurals 1–3 are slightly concave and form caudal processes in their dorsomedial

544   parts, at the level of pleural tubercles.

545   **Supramarginal scutes.** On each side of the carapace there were three elongated supramarginal

546   scutes (Figs 1–2, 4, 6A). The first supramarginal was pentagonal and had its longest tip directed

547   cranially. Caudally, this scute contacted the second supramarginal, and its dorsomedial tip was

548   tucked between the first and the second pleural scute. The second supramarginal was rectangular

549   and contacted the first supramarginal (cranially), the third supramarginal (caudally), and the

550 ventrolateral edge of the second pleural (dorsomedially). The third supramarginal was

551 pentagonal and shaped roughly the same as the first, but with its longest tip directed caudally.

552 This scute contacted the second supramarginal cranially and its dorsomedial tip was tucked

553 between the third and the fourth pleural scute. The row of three supramarginals always contacted

554 the bases of the fifth to ninth marginal ventrolaterally. The intersupramarginal sulci are located

555 roughly at the same level as the sulci separating the sixth, seventh, and eight marginal scute

556 areas, but some several millimeter misalignment frequently occurs – the intermarginal sulci

557 usually are shifted slightly cranially in relation to the intersupramarginal sulci (*Proterochersis*

558 *robusta* specimens SMNS 17561, Fig. 2G, SMNS 17755, and SMNS 18440, Fig. 2K; *P.*

559 *porebensis* specimens ZPAL V.39/8 (see Szczygielski & Sulej, 2019); ZPAL V.39/48, Fig. 4C–

560 D, ZPAL V.39/49, Fig. 4E–F, right side of ZPAL V.39/72, Fig. 4G, ZPAL V.39/160, and,

561 possibly, in ZPAL V.39/34, although the shell margin of that individual is damaged in that

562 region) but in some cases they may be shifted slightly caudally (left side of ZPAL V.39/72, Fig.

563 4G–H, ZPAL V.39/168). *P. porebensis* specimen ZPAL V.39/48 is closest to have these sulci

564 coinciding with only few millimeter cranial shift of intermarginal sulci (Fig. 4C–D). Other than

565 that, no meaningful variability or clear allometry was observed in the supramarginals. They seem

566 to increase their sizes more or less linearly with the carapace. The largest found supramarginal is

567 the first supramarginal of *Proterochersis porebensis* specimen ZPAL V.39/8 (see Szczygielski &

568 Sulej, 2019), which was 8 cm long and 5.5 cm high – slightly larger than in ZPAL V.39/49 (7.7

569 cm x 5 cm) and significantly larger than in ZPAL V.39/48 (6.6 cm x 4.2 cm) and ZPAL V.39/72

570 (6.7 cm x 4.2 cm). Unfortunately, the first supramarginal is too severely damaged in ZPAL

571 V.39/34 to allow precise measurement, but the probable outline of this scute on the right side of

572 the specimen suggests the length of approx. 4.2 cm. This would mean that, even more so than for

573 the ninth marginal, there is a good correlation between the length of the shell and the length of

574 the first supramarginal (Pearson correlation coefficient = 0.994 for n = 4). Based on that, the

575 shell of ZPAL V.39/8 may be estimated to be over 50 cm long.

576 **Marginal scutes.** There were two rows of marginals spanning from the craniolateral region of

577 the cervical scute to the caudolateral limits of the caudal notch (Figs 1–5, S5). Typically, each

578 row included fourteen scutes. Besides some minor random variations in shape and relative size,

579 which are usually difficult to grasp, the marginal scutes of *Proterochersis* spp. exhibited

580 variability in three main ways.

581   Firstly, their number was variable – variants of 15 marginals (ZPAL V.39/48 – possibly a

582   supernumerary abnormality) and 14 marginals (all the other specimens with complete marginal

583   series) are known (see Szczygielski & Sulej, 2016). There are at least 12 marginals identifiable

584   in the juvenile ZPAL V.39/34, but their exact number is uncertain due to preservation, so it is

585   probable that the typical number of 14 marginals was present. The layout relative to pleurals and

586   supramarginals suggests that one intermarginal sulcus is likely to be undetected in the bridge

587   region, below the supramarginal row, and this area is heavily damaged on both sides of ZPAL

588   V.39/34. Another likely missing sulcus should be located craniolateral to the cervical scute and

589   should delineate the first marginal. This area, however, is well-preserved in ZPAL V.39/34. It is,

590   nonetheless, possible that the scute was there, but its sulcus is too subtle to be identified (many

591   sulci on that specimen are very weak, see below) or that in such a young animal the scute was

592   very small and located at the very edge of the carapace – possibly the first marginal exhibited

593   allometry during development. This option seems plausible mainly because there is no nuchal

594   notch in ZPAL V.39/34 (the cranial edge of the carapace is flush – Fig. 4A–B, see also Sulej,

595   Niedźwiedzki & Bronowicz, 2012; Szczygielski & Sulej, 2016) in some specimens (particularly

596   SMNS 17561, Fig. 2F, ZPAL V.39/48, Fig. 4C, ZPAL V.39/49, Fig. 4E, and on the right side of

597   ZPAL V.39/72, Fig. 4G) the first marginal scute was almost entirely cranial to the cervical scute

598   (and, optionally, to the second marginal), having very little or no contact with the first vertebral

599   scute. This leaves two possibilities – either the first marginal scute was in some individuals

600   "crowded out" during ontogeny by the cervical and the second marginal or, at least in some

601   individuals, it started to develop on the very margin of the shell. Alternatively, some variability

602   in the number of marginal scutes is possible. Note that this condition is different from the

603   missing first marginal of *Keuperotesta limendorsa* – in *K. limendorsa* the lateral contact between

604   the cervical scute and the marginal series is very narrow or nonexistent (Szczygielski & Sulej,

605   2016), while in ZPAL V.39/34 it is wide. The smallest fragmentary specimen with the first

606   marginal craniolateral to the cervical scute is ZPAL V.39/390 (Fig. S1L–M).

607   The second type of marginal variability of *Proterochersis* spp. affects the layout of the

608   intermarginal sulci relative to the sulci of the remaining scutes, resulting in (usually minor)

609   differences of contacts between these scutes and variation of their shape. The first marginal in

610   dorsal aspect always contacted the cervical caudomedially, was subtriangular or trapezoidal,

611   depending on whether it was prevented from the contact with the first vertebral by the lateral tips

612   of the cervical scute (as in *P. porebensis* ZPAL V.39/48, Fig. 4C, ZPAL V.39/49, Fig. 4E, ZPAL

613   V.39/57, Figs S1N, S3B, and ZPAL V.39/72, Fig. 4G) or not (as in *P. robusta* SMNS 17561,

614   Fig. 2F, and SMNS 17930, Figs 2I, 6B–C, and *P. porebensis* ZPAL V.39/22, Fig. S3A),

615   respectively, and had a rounded craniomedial tip. In ventral aspect, it was subtriangular and had

616   a concave base. In this aspect, the intermarginal sulci of this and the following nine marginals as

617   well as the basal sulci of all except the first marginal are gently convex. The second marginal

618   was subrectangular to trapezoidal both in dorsal and in ventral aspect, always contacted the first

619   vertebral, in some specimens its tip touched the cervical (*P. porebensis* ZPAL V.39/48, ZPAL

620   V.39/49, ZPAL V.39/57, and ZPAL V.39/72), and in ZPAL V.39/57 (Figs S1N, S2B) it also

621   touched the first pleural. Consequently, in most *Proterochersis* spp. specimens the third marginal

622   scute was pentagonal in dorsal aspect (subrectangular in ventral aspect) and contacted both the

623   first pleural and the first vertebral scute (Figs 2, 4), but ZPAL V.39/57 (Fig. S1N, S3B) is the

624   only known exception – the sulcus between the second and the third marginal scute in that

625   specimen is continuous with the sulcus between the first vertebral and the first pleural scute, and

626   the third marginal was subrectangular in dorsal aspect. The fourth marginal was always

627   subrectangular in both aspects and contacted the first pleural in dorsal aspect and cranial part of

628   the axillary in ventral aspect. The fifth marginal was always pentagonal both in dorsal ventral

629   aspect, and contacted both the first pleural and the first supramarginal dorsomedially, and the

630   axillary and the first inframarginal scute ventromedially. In dorsal aspect, the marginals sixth to

631   eighth always contacted the row of three supramarginals and were subrectangular to weakly

632   pentagonal (depending on how much their intermarginal sulci are offset from the

633   intersupramarginal sulci, see above). In ventral aspect, they are usually pentagonal and contact

634   the row of four inframarginals. The caudal sulcus of the sixth marginal in this aspect is located

635   around the level of the sulcus between the first and the second inframarginal – in *P. robusta*

636   specimen SMNS 17561 (Fig. 3F) and *P. porebensis* specimen ZPAL V.39/48 (Fig. 5B) it is

637   slightly caudal, but seems to be slightly cranial in ZPAL V.39/49 (although the exact

638   morphology is obscured in that individual by damage, Fig. 5C), and it falls on a gap between the

639   inframarginals in *P. robusta* SMNS 18440 (Fig. 3H) and in *P. porebensis* ZPAL V.39/21 (see

640   below). The caudal sulci of the seventh and the eighth marginal fall around the midlengths of the

641   third and the fourth inframarginal, respectively. The ninth marginal was pentagonal in dorsal

642   aspect and subpentagonal in ventral aspect, gradually increasing its size caudally. It contacted the

643 third supramarginal dorsomediocranially, and the third pleural dorsomedially. The ventromedial

644 edge was gently curved rather than angular, it contacted the fourth inframarginal and formed the

645 caudal end of the bridge. The tenth marginal was pentagonal in dorsal aspect and subrectangular

646 in ventral aspect. Dorsomedially, it contacted the third and the fourth pleural. In most cases, the

647 dorsomedial sulcus of the tenth marginal is roughly continuous with the dorsomedial sulcus of

648 the ninth marginal, although in *P. porebensis* specimen ZPAL V.39/49 (Fig. 4E–F) these sulci

649 are set at an angle. A similar, but less pronounced break in sulcus direction is also present in *P.*

650 *robusta* specimen SMNS 17561 (Fig. 2G) and *P. porebensis* ZPAL V.39/72 (Fig. 4G–H). The

651 11th marginal was always subrectangular both in dorsal and in ventral aspect and dorsomedially

652 it contacted the fourth pleural. The 12th marginal was either trapezoidal (dorsomedial contact

653 with fourth pleural only – *P. robusta* SMNS 17561, Figs 2F–G, S5B, *P. porebensis* ZPAL

654 V.39/48, Figs 4C–D, S5H) or pentagonal (dorsomedial contact with the fourth pleural and the

655 fifth vertebral – remaining specimens, Figs 2, 4, S5) in dorsal aspect due to the varied position of

656 the sulcus between the 12th and the 13th marginal relative to the sulcus between the fourth pleural

657 and the fifth vertebral scute area (see Szczygielski & Sulej, 2016). In SMNS 17561 (Figs 2F–G,

658 S5B), ZPAL V.39/48 (Figs 4C–D, S5H), ZPAL V.39/72 (Figs 4G–H, S5K), and ZPAL V.39/386

659 (Fig. S5N) these sulci are located nearly in the same line (the intermarginal sulcus usually only

660 slightly caudal, but on the left side of SMNS 17651 even slightly cranial), while in SMNS

661 17755a (Figs 2H, S5C) and ZPAL V.39/49 (Fig. S5I) the pleurovertebral sulcus falls close to the

662 middle of the 12th marginal, and the intermarginal sulcus is located clearly more caudally. This is

663 also the configuration of sulci in the corresponding region of ZPAL V.39/34 (Figs 4A–B, S5G),

664 regardless of the number of marginals in that specimen. In SMNS 17930 (Figs 2I–J, 6A), the

665 sulcus between the last pleural and the last vertebral lies approximately in the same line as the

666 intermarginal sulcus between the 12th and the 13th marginal but the pleurovertebral sulcus in that

667 specimen is fully contained in the area restored with plaster and has an unusual layout (it is

668 continuous with the sulcus between the last pleural and the fourth vertebral instead of creating an

669 angle, as in other specimens – compare Figs 2 and 4), so it seems more plausible that in life it

670 met the 12th marginal in the middle. Given the limited sample which still exhibits some variance

671 in the relative position of sulci, it is possible that these two morphologies are not the only

672 possibilities, but a full spectrum of intermediate morphologies existed in the population.

673 Regardless of the shape of the 12th marginal, the 13th marginal was always subtrapezoidal in

674   dorsal aspect, had a convex rim, and contacted the fifth vertebral dorsomedially (in SMNS

675   17561, Figs 2F–G, S5B) and ZPAL V.39/48 (Figs 4C–D, S5H) additionally touching the caudal

676   end of the fourth pleural). Both the 12th and the 13th were subrectangular in ventral aspect. In

677   most specimens, the 14th marginal is the last of the series and in subadult and adult specimens it

678   had a rounded or spiky rim, the end of which was free from the preceding marginal. In ZPAL

679   V.39/48 this morphology is exhibited by the 15th marginal, while 14th is intermediate between the

680   15th and the 13th (Figs 4C–D, S5H). In some specimens (ZPAL V.39/6, Fig. S3D, ZPAL

681   V.39/18, Fig. S5E, ZPAL V.39/48, Fig. S5H) the sulcus between the last and second-to-last

682   marginal is sinuous. The notch between the last two marginals in most specimens (except ZPAL

683   V.39/23, Fig. S5D, ZPAL V.39/72, Fig. S5K, and ZPAL V.39/380, Fig. S5M) is rounded and the

684   bone around the level of the sulcus or just caudal to it is thinner than in the middle of the

685   marginal areas. Dorsomedially, the 14th and the 15th marginal (if present) contacted only the fifth

686   vertebral.

687   The caudalmost marginals (be it the 14th or the 15th) grew in a characteristic manner. In

688   *Proterochersis porebensis* specimen ZPAL V.39/34 (Fig. S5G) and in *P. robusta* specimen

689   SMNS 17561 (Fig. S5B) the last pair of marginals was small and triangular (they lacked a

690   caudoventral tip on their rims), broader then long (in ZPAL V.39/34 2.1 cm wide, measured

691   along the sulcus with the last vertebral and 1 cm long in the longest place; not measured in

692   SMNS 17561), and their edge was continuous with the edge of the preceding pair, resulting in

693   lack of serration (see also Szczygielski & Sulej, 2016). *P. porebensis* ZPAL V.39/23 (Fig. S5F)

694   is the smallest last marginal that has a tip, resulting in its roughly rhomboidal shape. It is 1.6 cm

695   wide, its maximal size (measured from the tip to the corner of the sulci with the fifth vertebral

696   and preceding marginal) is 1.9 cm, and length (from the sulcus with the fifth vertebral to the tip,

697   parallel to the caudal edge) is 1.4 cm (although the tip is broken, so these measurements should

698   probably be about 1 mm larger). Slightly larger (last marginal 2.1 cm wide, 2 cm long, 2.4 cm

699   max. size) *P. porebensis* individual, ZPAL V.39/18 (Fig. S5E), exhibits a transitional

700   morphology linking these small specimens and the more adult-like morphology – there is a small

701   but distinct tip and a shallow but noticeable rounded notch separates it from the rim of the

702   preceding marginal. In larger (and, supposedly, older) individuals, the last marginals were

703   becoming spikier, and longer than wide. The largest last marginal found thus far is in

704   *Proterochersis porebensis* specimen ZPAL V.39/59 (Fig. S5J; its width is 3.2 cm, maximal size

705   is 5.1 cm, and length is 3.9 cm). The remaining caudal marginals in large specimens, as

706   evidenced by ZPAL V.39/6 (Fig. S5D) and ZPAL V.39/59 (Fig. S5J), also tended to increase

707   their sizes towards the periphery of the shell, but lacked the serration and spikiness of the last

708   marginal.

709   One of the largest fragmentary *Proterochersis porebensis* specimens, ZPAL V.39/60 (Fig. S1O–

710   P), has the ninth marginal 7.8 cm long (measured on the external side of carapace, close to the

711   edge). ZPAL V.39/34 has this marginal approximately 3.5 cm long, ZPAL V.39/48 – 5.2 cm

712   long, ZPAL V.39/49 – 6.5 cm long, and ZPAL V.39/72 – 6 cm long. There seems to be

713   reasonably good correlation between the length of carapace (see above) and the length of that

714   element (Pearson correlation coefficient = 0.986 for n = 4). Based on that, the shell of ZPAL

715   V.39/60 may be estimated to reach up to about 60 cm in length.

716   **Scute sulci and surface.** The morphology and size of sulci in carapaces of *Proterochersis* spp. is

717   dependent on their ontogenetic age, as inferred from shell size and morphology. There is a

718   positive correlation between the size of the animal and the depth and breadth of sulci. In ZPAL

719   V.39/34 (Figs 4A–B, S4C, S5G) the sulci on the carapace are less than 1 mm wide and in some

720   cases one edge of the sulcus (e.g., the caudal edge of the vertebral scute area in intervertebral

721   sulci) is slightly curved externally, creating a characteristic lip and making it a bit higher than the

722   other edge (rarer is the situation when both the edges are raised, as in ZPAL V.39/2, Fig. S4A).

723   Also in ZPAL V.39/34, some sulci (e.g., between some lateral marginals) are very poorly

724   defined or seem to be bulging rather than sunken (e.g., between the cervical and the cranial

725   marginals or between the supramarginals) – the latter morphology may be a combination of the

726   two former, i.e., the sulcus proper (the groove) is too weak to be seen, but the lip around the

727   periphery of one of the scutes is visible. In larger specimens the sulci are broader (over one

728   centimeter in ZPAL V.39/63, Fig. S1B) and always sunken. The intervertebral and intermarginal

729   sulci usually have their cranial edge (formed by the preceding scute area) slightly higher than the

730   caudal one (formed by the succeeding scute area), but the edges are usually rounded and rarely

731   form a curved lip (e.g., ZPAL V.39/169, Fig. S4E; see also peripherals and costals figured in

732   Szczygielski & Sulej, 2019).

733   Most scute sulci on the carapace of *Proterochersis* spp. are sinuous (undulating; Fig. S8A–B, E–

734   G). This, however, seems to be at least partially determined by the size of the individual – in

735   probable juveniles, such as SMNS 16603 (Fig. 2D–E) and ZPAL V.39/34 (Figs 4A–B, S4C,

736   S5G), the sulci appear to be straight, and with age their undulation increases. It is most

737   prominent around the supramarginals and pleurals (Fig. S8A–B). The undulation is also related

738   to the radial striation on the surface of the scutes (Fig. S8A–B, E–F), which is frequently visible

739   (although usually faint) as imprints on the bone surface. The surficial striation and the undulation

740   of sulci are most prominent in the carapaces of the largest specimens, such as SMNS 16442,

741   ZPAL V.39/49 (Fig. 4E–F), ZPAL V.39/59 (Fig. S5J), and ZPAL V.39/63 (Fig. S1B), because

742   the frequency of the undulations seems to decrease and the depth of the striations as well as the

743   amplitude of the undulations seem to increase with growth (Fig. S8G). The striation on the

744   pleurals is most prominent along their cranial and pleuromarginal sulci (Fig. S8A–B), where the

745   grooves are longer than along the caudal and pleurovertebral sulci. Most marginals of not very

746   large individuals exhibit weak undulation of sulci and striation, with the exception of the ninth

747   marginal, in which these characters are strongly expressed along the sulcus with the third

748   supramarginal. Usually, the intervertebral sulci do not undulate (even though the pleurovertebral

749   sulci and the craniolateral sulcus of the first vertebral scute are clearly sinuous and, especially the

750   latter, frequently exhibit striation), but in very large individuals (e.g., ZPAL V.39/63, Fig. S1B)

751   the intervertebral sulci are becoming slightly uneven. Separate from the radial striation are the

752   bowed, concentric growth marks (Fig. S8A–F). These marks are located in the same areas as the

753   radial striation (most notably on pleurals along the cranial pleural and pleuromarginal sulci and

754   on vertebrals along the pleurovertebral sulci and along the craniolateral sulcus of the first

755   pleural), but are parallel rather than perpendicular to the scute sulci, usually fainter, broader, and

756   less densely packed. They do not reach the borders of the scute, and thus are not correlated with

757   the undulation of the sulci. Their relatively large breadth and shallowness makes them difficult to

758   spot on supramarginals and on the caudal and dorsomedial parts of the pleurals. Together with

759   their low number even in large specimens (no more than five pronounced growth marks per scute

760   are observed in available material) and their absence in young specimens, this also indicates that

761   they do not exhibit strict seasonal (annual) iterativity, but rather developed as a result of long-

762   term (polyseasonal) changes of environmental conditions. Both the radial striations and the

763   growth marks seem to originate near the caudodorsomedial region of the pleurals, where the

764   bone is thickened to a boss. This agrees with the observed pattern of scute growth (see below). A

765   similar boss is also present in some specimens in the caudodorsomedial region of the first

766 supramarginal, near the dorsomedial edge of the second supramarginal, and in the
767 craniodorsomedial region of the third supramarginal.

768 *Proterochersis robusta* specimen SMNS 17930 (Figs 2I, 6, S8D) is unique in its accentuated
769 growth marks of its vertebral and pleural scutes. There are two generations of these abnormal
770 growth marks per scute and they are bilaterally symmetrical. In breadth and position they
771 resemble typical growth marks of other *Proterochersis* spp. specimens (such typical growth
772 marks are also present between and above the abnormal ones in SMNS 17930, Fig. 6) but they
773 are deeper (in that respect approximating sulci) and have sharper edges. Along the cranial edges
774 of the first and the third vertebral scute the growth marks of the older, higher positioned
775 generation are bilaterally continuous and take form of "fake sulci" by copying the shape of true
776 sulci in front of them (albeit in smaller scale, as evidenced by the first vertebral). They, however,
777 do not reach the edges of the scutes and do not connect to true sulci. Based on the fact that this
778 morphology is present only in this one, middle-sized specimen, we interpret it as pathological.

779

780 **Plastron**

781 **Small specimens.** Several fragmentary specimens of small plastral bones morphologically
782 resembling early stages of plastra development in modern turtles are known from the
783 *Proterochersis* spp.-yielding localities of Murrhardt and Poręba – SMNS 81917 (Fig. S6A),
784 ZPAL V.39/165, ZPAL V.39/197 (Fig. S6C), ZPAL V.39/277 (Fig. S6B), ZPAL V.39/383,
785 ZPAL V.39/384 (Fig. S6D), and several other specimens from Poręba. Given their size (less than
786 8 centimeters each), it is likely that they belong to young juveniles, older than hatchlings but
787 younger than ZPAL V.39/34, which has its shell completely ossified. Other than the typical
788 characteristics of developing plastral bones – jagged edges with fingerlike projections and
789 minute striation indicative of progressing intramembranous ossification (e.g., Gilbert et al., 2001)
790 – they exhibit few superficial characters, no identifiable sulci, and only ZPAL V.39/165 and
791 ZPAL V.39/197 (Fig. S6C) can be identified with relative confidence as hyoplastra, based on the
792 shape of their incipient axillary buttresses. SMNS 81917 (Fig. S6A) is up to 2 mm thick and has
793 a rounded notch, which indicates that it is either a hyoplastron or a hypoplastron. Unfortunately,
794 it is exposed only in visceral view and flattened, therefore it is difficult to determine the

795   anatomical orientation of that specimen with full confidence. For that reason, it is also difficult to

796   identify it more precisely. A lip along one of the edges of the notch and gentle thickening along

797   the other edge differentiate this specimen from ZPAL V.39/165 and ZPAL V.39/197, potentially

798   hinting that it is a hypoplastron. Based on the overall shape and relatively large thickness (5 to 8

799   mm, compared to 1 to maximally 5 mm of ZPAL V.39/165 and ZPAL V.39/197), ZPAL

800   V.39/277 is likely a xiphiplastron (compare to, e.g., Zangerl, 1939; Gilbert et al., 2001; Rice et

801   al., 2016) or may be one of the mesoplastra – it is thicker than ZPAL V.39/165 and ZPAL

802   V.39/197, even though they are larger and relatively well-developed, so it is unlikely that this

803   element represents a hyoplastron at an earlier developmental stage, and for the same reason its

804   identity as a hypoplastron may be likely refuted. Overall, the developing plastral bones which

805   may be attributed to *Proterochersis* spp. are already more similar to plastral bones of derived

806   turtles than to fusing gastralia, from which the plastron is thought to have originated originated

807   (Schoch & Sues, 2015, 2017).

808   **Gular and extragular scutes.** *Proterochersis* spp. had a pair of gular (roughly pentagonal in

809   ventral view) and extragular (roughly trapezoidal in ventral view) scutes located at the cranial

810   end of the plastron (Figs 1, 3, 5, 7, S8), contacting the cranial edges of the humeral scutes (the

811   exception being *P. porebensis* ZPAL V.39/385, see below). The caudal sulci of the gulars are

812   roughly straight or gently concave and skewed craniolaterally, while the caudal sulci of the

813   extragulars are gently convex and skewed caudolaterally. Usually, the gulars are separated from

814   the extragulars by a tilted, craniolaterally directed sulcus, but the angle of tilting varies between

815   specimens and in SMNS 16603 the sulcus is directed craniocaudally. It appears that the size of

816   gulars relative to extragulars is variable – e.g., in ZPAL V.39/48 they are, respectively, 2.6 cm

817   and 3.2 cm wide, while in ZPAL V.39/385, 1.9 cm and 3.9 cm wide (measured cranially).

818   The shape of the gulars and extragulars shows large variability, some (but not all) of which may

819   be explained by the ontogeny. In smallest (and, supposedly, youngest) specimens, such as

820   *Proterochersis robusta* SMNS 16603 (Figs 3E, S7B) and *P. porebensis* ZPAL V.39/34 (Figs 5A,

821   S7E–G) these scutes were nearly completely flat ventrally (their ventral surface was flat and

822   more or less parallel to the humerals behind them) and the cranial edge of the cranial plastral

823   lobe was nearly flush (see Szczygielski & Sulej, 2016). In all specimens larger than SMNS

824   16603 and ZPAL V.39/34, the gulars and extragulars had cranial or craniolateral tubercle-like

825   projections, due to their length in lateral parts increasing proportionally faster than in the medial

826   parts, resulting in characteristically scalloped cranial edge of the cranial plastral lobe and the

827   gulars typically ending in a rounded point (Figs 3, 5, 8, S7). This character seems to be clearly

828   related to the size of the individual. This craniolateral expansion is accompanied by thickening of

829   the gulars (most prominent craniomedially). In *Proterochersis robusta* specimens that preserve

830   this region (CSMM uncat., Figs 3A, S7A; SMNS 16442, Fig. 3D; SMNS 17561, Figs 3F, S5C–

831   D; ZPAL V.39/388, S5K′–M′) the gulars and extragulars (in case of SMNS 17561, the only one

832   preserving these scutes) remain relatively flat, only gently bulged ventrally. In most *P.*

833   *porebensis* specimens, however, the gulars are significantly thickened in their craniomedial parts,

834   so most of their ventral surface is skewed caudolaterodorsally (ZPAL V.39/48, Figs 5B, S7H–J;

835   ZPAL V.39/49, Figs 5C, S7K–M; ZPAL V.39/187, Fig. S7R–T; ZPAL V.39/189, Fig. S7U–X;

836   ZPAL V.39/333, Fig. S7Y–A′; ZPAL V.39/379, Fig. S7B′–D′; ZPAL V.39/387, Fig. S7H′–J′;

837   ZPAL V.39/388, Fig. S7K′–M′; ZPAL V.39/420, Fig. S7N′–P′; see also Articles S2–S3). In

838   ZPAL V.39/187 (Fig. S7R–T) the gular was apparently relatively narrow and its point was

839   located around its mid-section rather than closer to the lateral border of the scute, resulting in

840   seemingly lower angle between the gular projections – the specimen is, unfortunately,

841   incomplete, so its exact orientation is uncertain. ZPAL V.39/385 (Figs 7, S7E′–G′) differs from

842   the remaining specimens in that its gulars are rounded ventrally and cranially. The preserved

843   medial parts of gulars of SMNS 16442 (Fig. 3D) are flat and proportionally thin despite its

844   relatively large size, but this may be caused by the compaction and/or related to the fact that in

845   that specimen the epiplastra, which formed a large section of the gular tubercles, are missing

846   (Szczygielski & Sulej, 2019).

847   The extragulars in the specimens larger than SMNS 16603 and ZPAL V.39/34 tend to lose their

848   alignment with the humerals, and instead become inclined more ventrally (i.e., towards the

849   external surface of the plastron; note that the cranial plastral lobe itself was bent more or less

850   dorsally, so in life this ventral inclination of the extragulars relative to the humerals resulted in

851   their free ends pointing predominantly cranially rather than ventrally; see Fig. 1B). The angle

852   between the cranial end of the humeral scute and base of the extragular scute at the level of the

853   extragulohumeral sulcus is variable, in some specimens being low (e.g., ZPAL V.39/49, Figs 5C,

854   S7K–M; ZPAL V.39/333, Fig. S7Y–A′), but much more distinct in others (e.g., ZPAL V.39/385,

855   Figs 7, S7E′–G′; ZPAL V.39/387, Fig. S7H′–J′). In addition to the angle at the base of the

856   extragular, the extragular exhibits various degrees of ventral curvature (the dorsal surface is

857   convex dorsally, the ventral surface concave ventrally). In some specimens (e.g., SMNS 17561,

858   Figs 3F, S5C–D; ZPAL V.39/333, Fig. S7Y–A′; ZPAL V.39/385, Figs 7, S7E′–G′; ZPAL

859   V.39/388, Fig. S7K′–M′) this curvature is minimal or virtually absent and thus, if the angle

860   between the base of the extragular and the humeral was also low, the cranial end of the

861   extragular was only slightly turned ventrally (e.g., ZPAL V.39/333, Fig. S7Y–A′; ZPAL

862   V.39/388, Fig. S7K′–M′). In other specimens the curvature is much more prominent and as a

863   result the angle between the tip of the extragular and the cranial portion of the humeral

864   approximated 70° (e.g., ZPAL V.39/48, Figs 5B, S7H–J; ZPAL V.39/49, Figs 5C, S7K–M;

865   ZPAL V.39/387, Fig. S7H′–J′). The downward curve of the extragulars may be easily explained

866   by their growth pattern (the dorsal part of the scute growing faster than the ventral part), hinting

867   that it was acquired with age. There is, however, no correspondence between the size of the

868   individual and the angle between the extragular tip and the humeral – ventrally flat extragulars

869   set at a low angle relative to the humeral are found both in small (e.g., ZPAL V.39/388, Fig.

870   S7K′–M′) and large (e.g., ZPAL V.39/187, Fig. S7R–T; ZPAL V.39/333, Fig. S7Y–A′)

871   individuals. Likewise, large angle between the extragular tip and the humeral is present both in

872   small (ZPAL V.39/387, Fig. S7H′–J′) and large (ZPAL V.39/49, Figs 5C, S7K–M) specimens.

873   This independence from the individual size may point at sexual dimorphism, but The PCA plots

874   and the regression analyses performed by us do not support that interpretation, suggesting that

875   the observed range of morphologies represents an intraspecific variability instead (see below).

876   The extragulars also differ in the shape of their craniolateral edge, which ranges from a

877   pronounced point (most evident in ZPAL V.39/420, but also present in ZPAL V.39/48, Figs 5B,

878   S7H–J; ZPAL V.39/49, Figs 5C, S7K–M; ZPAL V.39/186, Fig. S7N–Q; and ZPAL V.39/379;

879   Fig. S7B′–D′). In ZPAL V.39/187 (Fig. S7R–T), ZPAL V.39/333 (Fig. S7Y–A′), ZPAL

880   V.39/385 (Figs 7, S7E′–G′), and ZPAL V.39/388 (Fig. S7K′–M′) the angle between the cranial

881   and the lateral edge of the extragular is closer to 90°. In ZPAL V.39/387 (Fig. S7H′–J′) these

882   edges meet at an obtuse angle, like in juveniles.

883   The gular and extragular tubercles of *Proterochersis robusta* known to date show less

884   pronounced features (thickening, ventral curvature, prominent craniolateral points of extragulars)

885   than those of *P. porebensis*. It remains unclear whether this is an artifact of a small sample (only

886   four specimens of *P. robusta* have this region preserved, including juvenile SMNS 16603 and

887   very incomplete CSMM uncat. and SMNS 16442) or if the more exaggerated morphologies in

888   adult specimens are an autapomorphy of *P. porebensis*.

889   In ZPAL V.39/49 (Fig. 5C, S7K–M) the gulars are laterally asymmetrical (the right one is 2.7 cm

890   wide while the left one is 2.4 cm wide) even though the intergular sulcus is located on the

891   midline of the cranial plastral lobe. In CSMM uncat. (Figs 3A, S7A) and SMNS 16603 (Fig. 3E,

892   S7B) this sulcus is slightly moved to the left. Only the right gular is preserved in these two

893   specimens, but it may be hypothesized that this also caused some minor asymmetry.

894   **Abnormal scute set.** *Proterochersis porebensis* specimen ZPAL V.39/385 (Fig. 7, S7E′–G′)

895   exhibits a scute abnormality. In this specimen, between the row of gulars and intergulars and the

896   set of humerals, there were paired, roughly triangular supernumerary scutes. The right one was

897   slightly smaller than the left one, and did not reach the lateral edge of plastron, allowing partial

898   contact between the right extragular and humeral. The left, larger supernumerary scute did reach

899   the edge of the plastron, and thus separates the extragular from the humeral completely. The

900   sulci separating these two additional elements from the humerals have slightly raised edges, are

901   deepest medially, and become less clear laterally. At first sight, their layout resembles the

902   caudolateral suture of the entoplastron, as visible in *P. robusta* specimen SMNS 16442 (Fig. 3D;

903   see Szczygielski & Sulej, 2019), but upon closer inspection, they cannot be mistaken for this

904   suture – their edges are smooth, they lack interdigitation and other macro- and microscopic

905   characteristic of sutures but instead their morphology is consistent with that of other sulci in that

906   specimen, they are located more caudolaterally than the entoplastral suture and do not enter the

907   area of gulars (nor extragulars), and there is no sign of sutures on the visceral surface of that

908   specimen.

909   **Humeral scutes.** *Proterochersis* spp. had a set of two humerals (Figs 1, 3, 5, 7, S7) located

910   caudal to the gulars and extragulars (except ZPAL V.39/385, see above) cranial to the pectorals.

911   The caudal sulci of the humeral set have a characteristic appearance – their lateral ends are

912   turned cranially, and medial ends are usually turned more or less caudally, forming a variably

913   pronounced tip (best visible in *P. robusta* specimens CSMM uncat., Fig. 3A, and SMNS 17561,

914   Fig. 3F, as well as in *P. porebensis* specimen ZPAL V.39/49, Fig. 5C). Besides ZPAL V.39/385,

915   which had the craniomedial edges of the humerals misshaped due to presence of an additional

916   abnormal scute pair, there is no clear variability in humeral shape.

917   **Axillary scutes.** There was a pair of elongated, hexagonal axillary scutes present in

918   *Proterochersis* spp. Each contacted the ventromedial bases of the fourth and fifth marginal, the

919   cranial border of the first inframarginal, and the cranial edge of the lateral part of the pectoral

920   scute. Best preserved in *Proterochersis robusta* SMNS 17561 (Fig. 3F) and *P. porebensis* ZPAL

921   V.39/48 (Fig. 5B), these scutes do not exhibit visible variation.

922   **Pectoral scutes.** There was a pair of pectoral scutes present in *Proterochersis* spp. (Figs 3, 5, 7).

923   Cranially, they contacted the humerals, their lateral ends contacted with the axillaries and the

924   first two pairs of inframarginals, and caudally they contacted the first pair of abdominal scutes.

925   The only specimen with an unusual shape of the pectorals is *P. robusta* specimen SMNS 17561

926   (Fig. 3F), in which the scutes were abnormally elongated caudally in the middle portion (see

927   below).

928   **Abdominal scutes.** There were two pairs of wide and short, strap-like abdominals in

929   *Proterochersis* spp. (Figs 1, 3, 5). The first pair was located between the pectorals (cranially), the

930   second and the third inframarginal (laterally), and the second pair of abdominals (caudally). The

931   latter, beside the first abdominal pair, contacted the third and fourth inframarginal and the ninth

932   marginal laterally, and the femoral scutes caudally. Both abdominal pairs gradually increased in

933   length towards the ventromedial end of the bridge, at which level their cranial sulci are

934   characteristically bent. From that point towards the lateral ends of the bridge, the length of the

935   first abdominal remained roughly constant and the length of the second abdominal slightly

936   decreased. Typically, abdominals of both pairs met medially. In *P. robusta* specimen SMNS

937   17561 (Fig. 3F), however, the first pair of abdominals lacked medial contact. These scutes

938   gradually decreased in length towards the midline and disappeared completely just before

939   reaching it. Their place in the mid-section of the plastron seems to be partially taken by the

940   caudal expansions of the pectorals and partially by the second pair of abdominals, which seem to

941   retain roughly constant length instead of tapering medially, as typical (compare Figs 3, 5, 7).

942   This morphology is known in only one individual out of at least five other specimens of *P.*

943   *robusta* and several specimens of *P. porebensis*. We consider it as an abnormality, although the

944   small sample size and retained symmetry make this assumption tentative. SMNS 15479 (a

945   double external mold of proterochersid plastron found in Reichenbach, Germany, figured but not

946   described by Gaffney, 1990, fig. 68 therein) lacks characters that would allow its precise

947   identification as *P. robusta,* but such an identity is possible, in which case it would further

948   support the medial contact of the first pair of abdominals as the norm.

949   **Inframarginal scutes.** *Proterochersis* spp. had four polygonal or rounded inframarginal scutes

950   on each side (Figs 1, 3, 5). Dorsolaterally, they contacted the marginal row (fourth to eighth

951   marginal, see above). Cranially, the first inframarginal contacted the axillary scute.

952   Ventromedially, the inframarginals contacted the lateral ends of the pectoral (first and second

953   inframarginal), the first abdominal (second and third inframarginal), and the second abdominal

954   (third and fourth inframarginal) scute. In ZPAL V.39/34 (Fig. 5A), the inframarginals were

955   relatively narrow, elongated, and comma-shaped. In larger specimens (SMNS 17561, Fig. 3F;

956   SMNS 17755, Fig. 3G; SMNS 18440, Fig. 3H; ZPAL V.39/48, Fig. 5B; ZPAL V.39/49, Fig. 5C)

957   they increasingly gained girth, becoming relatively flatter. In *Proterochersis robusta* specimen

958   SMNS 17755 (Fig. 3G) the third and the fourth inframarginal are separated by a small gap. In *P.*

959   *robusta* specimen SMNS 18440 (Fig. 3H) there is a triangular gap between the cranial part of the

960   third inframarginal and the seventh marginal, and possibly there was a gap between the first

961   inframarginal, the sixth and the seventh marginal, and (maybe) the second inframarginal, but the

962   caudal part of the first marginal is damaged, making this uncertain. In *P. porebensis* ZPAL

963   V.39/21 there also is an apparent gap between the first and the second inframarginal, around the

964   level of the sulcus between the fifth and the sixth marginal. These gaps seem to lack any pores

965   inside, so they likely were interplates covered by skin rather than housed Rathke's glands,

966   especially since there is no evidence of similar gaps in the remaining specimens of

967   *Proterochersis* spp.

968   **Femoral scutes.** The femorals in *Proterochersis* spp. were located caudal to the bridge, between

969   the second pair of the abdominal scutes and the anals (Figs 1, 3, 5). Typically, the

970   abdominofemoral sulcus is gently bowed caudally, and in most specimens (the exceptions being

971   *P. robusta* SMNS 16442, Fig. 3C, and *P. porebensis* ZPAL V.39/48, Fig. 5B) this is also true for

972   the femoroanal sulcus. Both of these sulci are always directed caudolaterally – the femoroanal

973   sulcus more profoundly than the abdominofemoral. No clear variability is observed in these

974   scutes.

975   **Anal scutes.** Contacting the femorals cranially and the intercaudal and caudal scutes caudally,

976   the anals of *Proterochersis* spp. were the longest scutes in the caudal plastral lobe (Figs 1, 3, 5).

977   They gradually decreased in width caudally. No clear variability was observed for these scutes.

978   **Intercaudal and caudal scutes.** The caudalmost part of the plastron, presenting a set of two

979   caudal and one intercaudal scutes, seems to be the most variable section of the shell in

980   *Proterochersis* spp. (Figs 1, 3, 5, 9). In the smallest specimens, such as ZPAL V.39/34 (Figs 5A,

981   9K) and ZPAL V.39/66 (Fig. 9J), the caudal processes are small, wider than long, and are

982   entirely (ZPAL V.39/34) or almost entirely (ZPAL V.39/66) covered dorsally by the caudal plate

983   of ischium. In larger specimens, the variation is expressed in several ways. Firstly, the caudal

984   processes may be relatively short and rounded distally (CSMM uncat., Figs 3A, 9A; SMNS

985   17561, Figs 3F, 9C; ZPAL V.39/69, Fig. 9F) or relatively long and spiky (SMNS 12777, Figs

986   3C, 9B; ZPAL V.39/48, Figs 5B, 9G; ZPAL V.39/49, Figs 5C, 9D; ZPAL V.39/56, Fig. 9L–N;

987   ZPAL V.39/68, Fig. 9H; ZPAL V.39/70, Fig. 9I; ZPAL V.39/71, Fig. 9E; ZPAL V.39/199, Fig.

988   9O–Q). Secondly, the lateral edges of the caudal processes are generally thinner than the medial

989   edges, but in ZPAL V.39/56 (Fig. 9N) and SMNS 12777 (apparently – the process is not

990   preserved, but it left an imprint in the rock matrix; Figs 3C, 11B) the lateral edge is sharpened,

991   while in the remaining specimens it is more rounded. In some cases, this may be an artifact of

992   preservation (the edges are frequently damaged), but some well-preserved and seemingly

993   undamaged specimens (most notably ZPAL V.39/68, Fig. 9H, and ZPAL V.39/199, Fig. 9Q)

994   show that the edge indeed was rounded in some individuals. Thirdly, in some large specimens

995   (ZPAL V.39/69, Fig. 9F; ZPAL V.39/70, Fig. 9I; ZPAL V.39/71, Fig. 9E; *P. robusta* specimens

996   are not prepared sufficiently to validate whether this is the case) the ischium is visible in ventral

997   view between the caudal processes, but in most specimens it is not exposed. The degree of this

998   exposure varies from minor (ZPAL V.39/70) to major (ZPAL V.39/69, ZPAL V.39/71).

999   Fourthly, the angle between the caudal processes varies – e.g., in ZPAL V.39/68 (Fig. 9H) it is

1000   low, in ZPAL V.39/49 (Figs 5C, 9D) and ZPAL V.39/70 (Fig. 9I) it is intermediate, and in

1001   ZPAL V.39/48 (Figs 5B, 9G) and ZPAL V.39/69 (Fig. 9F) it is larger. Finally, the size and the

1002   proportions (length to width) of the intercaudal scute is varied – e.g., in ZPAL V.39/68 (Fig. 9H)

1003   it is very elongated craniocaudally (2.2 cm in length x 1.2 cm in width), in ZPAL V.39/69 (Fig.

1004   9F) it is nearly as wide as long (2.3 cm in length x 2.2 cm in width), while in SMNS 56606 (Fig.

1005   3J) it seems to be wider than long (but unfortunately damaged). Because there is no clear

1006 correlation between these morphologies and size of the specimen, we decided to use shape

1007 analysis in search of possible sexual dimorphism (see the section shape analysis below, Fig. 9C–

1008 F).

1009 Based on the width of the caudal plastral lobe, *Proterochersis robusta* specimen SMNS 17561

1010 (Figs 3F, 9C) appears to be of roughly comparable size to *P. porebensis* specimen ZPAL

1011 V.39/66 (Fig. 9J), but the former has a well-developed, adult-like shell (e.g., no middorsal

1012 troughs and pronounced keel, cranially protruding gulars and extragulars, caudally protruding

1013 caudal processes), while the latter appears to be a juvenile, more similar to ZPAL V.39/34 (Figs

1014 5A, 9K) than to larger specimens, suggesting that *P. robusta* achieved adult-like features (and,

1015 supposedly, sexual maturity) at smaller sizes than *P. porebensis*. This is congruent with larger

1016 average and maximal sizes of *P. porebensis* specimens found thus far compared to *P. robusta*

1017 specimens.

1018 ZPAL V.39/200 (Fig. 9R–T) is a curious, thorn-like element with lamellar sutural surface at its

1019 base. It may represent an isolated caudal plastral process, although it is small compared to other

1020 specimens. Otherwise, it may be interpreted as a part of a complex cervical or caudal osteoderm,

1021 similar to those described by Gaffney (1990) for *Proganochelys quenstedti* Baur, 1887, and

1022 suggested by Lucas et al. (2000) and Joyce et al. (2009) for *Chinlechelys tenertesta* Joyce et al.,

1023 2009 (see discussion in Szczygielski & Sulej, 2019), but no other evidence of such osteoderms is

1024 known from Poręba nor German proterochersid-yielding localities.

1025

1026 **Shape analysis**

1027 No clustering was seen on the PCA plots of the gular region of the plastron, indicating an

1028 intraspecific variability (Fig. 8). The plot of regression scores (a projection of the shape of each

1029 specimen) versus log centroid size (linked to size) for the gular cross-sections shows no

1030 association between the shape and size (Fig. 8F). On the other hand, in the case of the gular and

1031 extragular shape in ventral view, the regression analysis shows shape change with the increasing

1032 size (Fig. 8E).

1033   In the in the PCA plot of the caudal processes and intercaudal scute (Fig. 10A) the principal

1034   component 1 (65.3% of total variance) connected to the elongation, slenderness, and spikiness of

1035   the caudal process. Increasing scores on PC2 (19.7% of total variance) show widening of the

1036   connection between the caudal process and the intercaudal scute. The likely juveniles (ZPAL

1037   V.39/34 and ZPAL V.39/66) have short and rounded caudal processes. Then, the specimens

1038   ZPAL V.39/69, CSMM, and SMNS 17561 placed around 0 value of PC1 and PC2 show longer

1039   and rounded caudal process. The most positive values of PC1 are occupied by specimens with

1040   very long and spiky caudal processes. In the second PCA plot (Fig. 10B), the PC3 shape changes

1041   are connected to the angle between the caudal process and the intercaudal scute and the

1042   specimens are placed similarly to former plot.

1043   To check whether the lengthening and sharpening of the caudal processes results from

1044   ontogenetic changes, we run a regression analysis (pooled by species, Fig. 10C) of two

1045   *Proterochersis* species. The results show that 56.9% (p-value < 0.001) of the total shape

1046   variability can be explained by size variation. The regression plot shows that specimens similar

1047   in size can possess short and rounded caudals (ZPAL V.39/48) or long and spiky (ZPAL

1048   V.39/69). The result suggests that these morphotypes of developed caudal processes are not a

1049   result of ontogenetic changes.

1050   We run a multivariate analysis of variance (MANOVA) for the group including the specimens

1051   with short and rounded caudals (ZPAL V.39/69, SMNS 17561, and CSMM uncat.) and the group

1052   containing the individuals with long and spiky caudals (ZPAL V.39/70, ZPAL V.39/71, ZPAL

1053   V.39/49, ZPAL V.39/48, and SMNS 12777). The MANOVA showed that they differ

1054   significantly in shape (F = 2.48, p-value < 0.01) but not in (centroid) size (F = 3.21, p-value >

1055   0.3; Table S6). Therefore, the difference in shape but not in size indicates that the dimorphism is

1056   not ontogenetic. Moreover, here is no significant distinction in the shape of caudal process

1057   between species (Table S6). It is possible that the that the differences are caused by the sexual

1058   dimorphism, but so far the sample size is too small to unambiguously confirm that.

1059   **Scute sulci and proportions.** Like in carapace, the width and depth of sulci increase with the

1060   size of the animal. Unlike in carapace, the sulci in plastron never seem to undulate and there is

1061   no scute striation. In large specimens, however, the sulci do exhibit some minor irregularities,

1062   while in small ones they are usually very straight (compare Figs 3, 5). As in modern turtles, there

1063   is typically some bilateral asymmetry when it comes to the sulci layout on the plastron – most

1064   notably, the scutes in corresponding pairs (humerals, pectorals, abdominals, etc.) differed slightly

1065   in length, so the points in which their cranial and caudal sulci meet the midline are shifted

1066   slightly cranially or caudally relative to each other (this is best visible in CSMM uncat., Fig. 3A).

1067   This shift is random, so there is no clear alteration (i.e., the sulci on one side do not always

1068   precede the sulci on the other side).

1069   **Plastron thickness.** The plastron in proterochersid is not equally thick throughout its length and

1070   width. It is thinnest in the bridge area and around midline, and thickest in the lateral sections of

1071   femoral scute area, where it forms a bulbous expansion. In ZPAL V.39/34 the femoral is 1.8 cm

1072   thick, in ZPAL V.39/48 it is 2.1 cm thick, and in ZPAL V.39/49 it is 2.5 cm thick. The thickest

1073   plastron found thus far is ZPAL V.39/157, with femoral scute region 2.7 cm thick in the lateral

1074   part and about 0.5 cm thick at the medial cranial section of the anal scute area.

1075

1076   Variation of shell features

1077   Scute surface

1078   **Radial striation.** Radial striation and sinuous sulci, similar to those observed in *Proterochersis*

1079   spp. (e.g., Fig. S8A–B, E–G), are present in numerous Triassic (de Broin et al., 1982; Gaffney,

1080   1990) and Jurassic (Broin, 1994; Anquetin & Claude, 2008; Anquetin & Joyce, 2014; Anquetin,

1081   Püntener & Billon-Bruyat, 2014; Jansen & Klein, 2014; Anquetin, Püntener & Joyce, 2017;

1082   Sullivan & Joyce, 2017) turtles. The same superficial characters are also present in *Keuperotesta*

1083   *limendorsa* specimen SMNS 17757, including clear striation and growth marks along the cranial

1084   and lateral edges of the last vertebral scute, and unlike *Proterochersis* spp. the sulcus between

1085   the fifth and fourth vertebral scute of *K. limendorsa* is clearly sinuous. In that specimen, these

1086   characters are more pronounced in the caudal part of the shell than in the cranial part, but this

1087   may be a preservation artifact. Due to small sample, it is unknown whether this is taxonomically

1088   important, or just related to an old ontogenetic age of SMNS 17757. The ecology of early turtles

1089   is controversial, but currently no clear adaptive value is apparent for these low, radial ridges, and

1090   given their widespread occurrence in early taxa, they are likely plesiomorphic. Moreover, a

1091 delicate striation is present on scutes of some turtles, and possibly in older specimens it may

1092 leave imprints on underlying bones.

1093 **Growth marks.** The presence of bow-shaped scute growth marks (e.g., Fig. S8A–F) is most

1094 typical for the turtle species in which the scutes are not shed (Zangerl, 1969; Alibardi, 2005).

1095 This most usually means terrestrial turtles, but there are also some examples of scute shedding

1096 terrestrial box-tortoises or non-shedding aquatic emydids (Alibardi, 2005). The non-pathological

1097 growth marks in *Proterochersis* spp. and *Keuperotesta limendorsa* are, however, very subtle, and

1098 more comparable to those seen in some specimens of scute-shedding aquatic turtles (e.g., *Emys*

1099 *orbicularis* (Linnaeus, 1758), *Mauremys caspica* (Gmelin, 1774); Szczygielski, pers. obs.),

1100 therefore it is not clear whether proterochersids shed their scutes. Furthermore, if scute shedding

1101 is an adaptation to aquatic environment (e.g., by lowering drag during swimming thanks to

1102 smoother shell surface or as a countermeasure against shell rot), it is possible that this

1103 mechanism developed with some delay. In such a case, the scute shedding could have been

1104 initially a rare (possibly abnormal) phenotypic trait, only subsequently promoted and eventually

1105 fixed by the natural selection some time after turtles invaded the aquatic environment, and thus

1106 might have been absent in the earliest aquatic testudinates. Conversely, if scute shedding is

1107 plesiomorphic for turtles and was repressed as an adaptation to terrestrial life (by thickening the

1108 durable, keratinous layer protecting the epidermis and shell bones), the inability of scute

1109 shedding might have also been selected and developed over time in more advanced terrestrial

1110 turtles. For that reason, the correlation between the scute shedding and life environment may not

1111 be strict for the earliest, Triassic turtles. The oldest (and, apparently, the only known) fossilized

1112 isolated turtle scutes were described from the Middle Jurassic of the United Kingdom, but they

1113 possess a very dense layout of growth marks and were interpreted as removed post-mortem from

1114 the turtle carcass rather than shed (Anquetin & Claude, 2008).

1115 **Middorsal ridges and keels.** A low middorsal ridge (e.g., Fig. S4C–E, G) was thus far reported

1116 among Triassic turtles only in *Proganochelys quenstedti* in the cranial portions of its vertebral

1117 scutes (Gaffney, 1990). A subtle ridge is also present crossing the area of the vertebral scutes

1118 (including the fifth vertebral) of *Keuperotesta limendorsa* specimen SMNS 17757. Similar low

1119 midline ridges are also present in numerous modern turtles (Pritchard, 2008). While the keels

1120 alone are relatively common also in young individuals of modern turtles (Ferreira, pers. comm.

1121 2018; Szczygielski, pers. obs.), given current data, it seems that deep troughs lateral to the keels

1122 are unique to young stages of shell development of *Proterochersis* spp. Their genesis and

1123 relationship to vertebral scutes, however, are problematic. Certainly, they are not caused by any

1124 post-mortem, mechanical folding, because they are symmetrical, their morphology is virtually

1125 the same in both specimens, and there is no sign of folding or cracking on the ventral surface of

1126 ZPAL V.39/2 (Fig. S4A–B). It would be tempting to conclude that in life they were covered by

1127 normal, unpaired vertebral scutes, and that the troughs were initially filled by dermis, connective

1128 tissue, or rudimentary muscles, and subsequently by developing bone of neurals. The walls of the

1129 troughs, including the lateral edges of the midline keel, bear, however, the same rough texture as

1130 the remaining, scute-covered surfaces of carapacial bones (contrary to some deeper-located or

1131 visceral surfaces, see Szczygielski & Sulej, 2019), suggesting that they were lined by keratinous

1132 elements as well. On the other hand, the scutes of larger and probably older specimens do not

1133 show any remnants of deep troughs in their older parts. This is problematic, because turtle scutes

1134 grow from the bottom (Alibardi, 2005) and the heavily cornified and stiff outer scute layers

1135 hardly seem to be susceptible to remodeling. This would call out either for local, temporal scute

1136 decornification of mid-sections of proterochersid vertebral scutes, as in plastra of breeding male

1137 chelonioids (Wibbels, Owens & Rostal, 1991; Wyneken, 2001; Pritchard, 2008), or for scute

1138 shedding in proterochersids, at least when young. Even with help of scute shedding, though,

1139 filling of the scute-lined troughs with bone still appears tricky, because the shape of the younger,

1140 deeper, and less cornified layer of the scute, which would potentially allow some flexibility and

1141 space for bone apposition, would still be determined by the older, stiffer, external layer. It seems,

1142 nonetheless, possible that uneven thickness of cornifying epidermis (thicker below the flat parts

1143 and thinner at the points of penetration into the troughs) would, with every generation of shed

1144 scutes, result in shallower troughs, and eventually in their disappearance. Less probable seems

1145 the hypothesis that the newer generations of scutes of *Proterochersis* spp. attained their stiffness

1146 some time after the older scutes were shed, and until then they were pliable enough to allow

1147 gradual filling of the troughs, or that the troughs are pathological and developed independently in

1148 two specimens of similar sizes from the same locality. Possibly, this conundrum will be solved

1149 by future histological studies. Until then, these interpretations remain speculative.

1150 **Plastron scutes.** The scutes of the plastron in proterochersids (but also in *Proganochelys*

1151 *quenstedti*) generally lacked undulating edges, superficial striation, and growth marks, in which

1152 they differ from the carapacial scutes. In agreement with this, the molecular background of

1153 plastral and carapacial scute development is divergent (Cherepanov, 1989; Moustakas-Verho et

1154 al., 2014; Moustakas-Verho & Cherepanov, 2015). These differing characteristics may result

1155 from different evolutionary history of plastron and carapace – they developed separately and the

1156 former appeared before the latter (Li et al., 2008; Schoch & Sues, 2015, 2017) – and possibly are

1157 rooted in varied (primaxial vs abaxial) environment of morphogenesis (Burke, 1989; Nowicki &

1158 Burke, 2000; Burke & Nowicki, 2003; Shearman & Burke, 2009).

1159

1160 **Scute anomalies and growth**

1161 Anomalies in scute layout, shape, and number are relatively frequent in turtles (Parker, 1901;

1162 Coker, 1905, 1910; Grant, 1936b; Młynarski, 1956; Zangerl & Johnson, 1957; Zangerl, 1969;

1163 Cherepanov, 2006, 2014, 2015; Farke & Distler, 2015; Sullivan & Joyce, 2017; Lichtig & Lucas,

1164 2017). Thus far, however, no unambiguous scute anomalies were reported in the Triassic turtles.

1165 The only possible exception is the missing first marginal in one of *Proganochelys quenstedti*

1166 specimens but interpretation of that case is uncertain (Gaffney, 1990; Szczygielski, 2017). Some

1167 of the morphologies described here were previously noted by Karl and Tichy (2000), but not

1168 considered in wider populational or developmental context, but rather glanced over as a part of

1169 normal intraspecific variation of their "*Murrhardtia staeschei*". The data on *Proterochersis* spp.

1170 presented here reveals, therefore, the first uncontroversial evidence of scute abnormalities in the

1171 Triassic turtle taxa.

1172 The most obvious cases concern additional scutes and improper scute shape. The asymmetry of

1173 the lateral parts of the first vertebral scute in ZPAL V.39/49, as well as the asymmetrical

1174 intervertebral sulci of *Proterochersis robusta* specimens CSMM uncat. and SMNS 17561, and *P.*

1175 *porebensis* specimens ZPAL V.39/34 and ZPAL V.39/72 are minor and may be easily explained

1176 as effects of uneven tempo of scute growth in its contralateral parts, and most likely are not

1177 caused by improper development (skipped segment or additional placode in vacant myoseptum)

1178 and fusion of scute placodes (Cherepanov, 1989, 2006, 2014, 2015; Moustakas-Verho et al.,

1179 2014; Moustakas-Verho & Cherepanov, 2015; Moustakas-Verho, Cebra-Thomas & Gilbert,

1180 2017). Likewise, the medial separation of the first pair of abdominal scutes in *P. robusta*

1181   specimen SMNS 17561 appears to be caused by simple overgrowth of the preceding and the

1182   succeeding pair of scutes. As noted by, e.g., Zangerl and Johnson (1957), abnormalities in the

1183   abdominals are relatively frequent. The supernumerary prehumeral scutes of *P. porebensis*

1184   specimen ZPAL V.39/385 are, on the other hand, a textbook example of an effect of additional

1185   pair of scute placodes. This specimen is even more interesting due to relative rarity of additional

1186   scutes in the plastron in many taxa (e.g., Newman, 1906b; Lynn, 1937), and rarity of bilateral

1187   additional scutes in general (e.g., Newman, 1906b; Coker, 1910; Młynarski, 1956; Moustakas-

1188   Verho & Cherepanov, 2015).

1189   *Proterochersis robusta* specimen SMNS 17930 differs from all the other *Proterochersis* spp.

1190   specimens in its abnormally deep growth lines which form "false sulci" along the cranial limits

1191   of vertebral scutes. They are well-visible on pleural and vertebral scute areas, and on the latter

1192   they are bilaterally symmetrical, which excludes trauma or post-mortem damage from the list of

1193   potential causes. Renal hyperparathyroidism (improper bone formation caused by calcium

1194   deficiency related to impeded vitamin D metabolism) was reported to cause accentuated

1195   'interplates' and growth lines (Frye, 1994; Rothschild, Schultze & Pellegrini, 2013). The

1196   morphology of SMNS 17930 may therefore be tentatively interpreted as resulting from this

1197   condition, but further studies will validate this diagnosis. Alternatively, if proterochersids did

1198   normally shed their scutes, the morphology of SMNS 17930 may be an effect of dysecdysis

1199   (scute retention). In any case, this specimen informs about the growth of scutes in *Proterochersis*

1200   spp.

1201   In modern turtles, newly cornified layers of the shell develop below the old scutes (Alibardi,

1202   2005). The scutes typically do not grow with equal speed in all directions, resulting in an off-

1203   center position of the oldest (embryonic) part relatively to whole scute area (Zangerl, 1969;

1204   Cherepanov, 2015). Based on the growth rings on the scute areas of *Proterochersis* spp.

1205   (including very clear abnormal growth marks of SMNS 17930) and *Keuperotesta limendorsa*, it

1206   can be inferred that in proterochersids this growth characteristics were also present. The vertebral

1207   scutes grew fastest cranially, moderately fast laterally, and slowest caudally. This is also true for

1208   the odd-shaped first vertebral, which apparently grew mainly cranially, while its caudal process

1209   retained throughout life the same general shape and size. The pleurals grew fastest cranially and

1210   lateroventrally, and their oldest areas were likely located close to (or on) the caudodorsomedial

1211   bosses. Based on the layout of striation (Gaffney, 1990), vertebrals and pleurals of
1212   *Proganochelys quenstedti* also grew predominantly cranially (not in a radially symmetrical way,
1213   contra Cherepanov, 2015). No growth marks are visible on supramarginals and marginals, but
1214   the striation of the first and the third supramarginal suggests that the embryonic areas were
1215   located, respectively, in the caudal and in the cranial region of the scute area (possibly slightly
1216   above the midline). Little can be said about the plastral bones, with the exception of gulars and
1217   extragulars, which apparently grew faster dorsally than ventrally, resulting in their ventral
1218   curving (see above).

1219   In the light of the above, the deep, sulci-like grooves in the cranial parts of vertebral scutes of
1220   *Proterochersis robusta* specimen CSMM uncat. and shallower, but similar positionally and
1221   morphologically depressions of SMNS 17930 and (even less pronounced) SMNS 17561 (Figs
1222   2F–G, 6) are best interpreted as appearing late in ontogeny. As stated above (see Results
1223   section), there is a positive correlation between the severity of this morphology and size of the
1224   specimen. It is highly unlikely that virtually the same (albeit pronounced with various severity)
1225   morphologies appeared ideally medially on several vertebrals of three individuals as a result of
1226   trauma or post-mortem damage. For that reason, we interpret this as a developmentally-driven
1227   scute splitting. Occurrences of splitting (i.e., partially divided) scutes were reported in modern
1228   turtles (e.g., Parker, 1901; Coker, 1910; Grant, 1936b; Zangerl & Johnson, 1957) and the split
1229   usually occurs in the youngest parts of the affected scutes (Coker, 1910; Grant, 1936a; Zangerl &
1230   Johnson, 1957). In some cases, this phenomenon may be explained as a result of damage to the
1231   epidermis between the scutes, which leads to scar formation and loss of proper cornification
1232   ability. In many cases, however, the splitting occurs in regions of asymmetry apparently caused,
1233   e.g., by pairing of vertebral scute primordia, originating from asymmetrically located scute
1234   placodes or just in the middle of a vertebral, and the split divides the areas of particular placodes
1235   (Coker, 1910; Grant, 1936b; see Cherepanov, 1989, 2006, 2014, 2015; Moustakas-Verho et al.,
1236   2014; Moustakas-Verho & Cherepanov, 2015; Moustakas-Verho, Cebra-Thomas & Gilbert,
1237   2017). Therefore, it seems that in some cases during postnatal life, due to unknown factors, the
1238   primarily fused scute placodes may lose connection and start to produce separate scutes. It is,
1239   nonetheless, possible, that the lateral integration between the vertebral placodes was relatively
1240   weak in early turtles such as *P. robusta* (it may be hypothesized that huge size of vertebrals may
1241   be partially responsible, e.g., by causing some signaling difficulties in large specimens; a mid-

1242 portion loss of coordination of cornification front may be also responsible for the asymmetry of
1243 the sulcus between the third and the fourth vertebral scute in CSMM uncat.), and for that reason
1244 the medial split was relatively common. Curiously, there is no sign of cranial vertebral scute
1245 splitting in any specimen of *P. porebensis* or *Keuperotesta limendorsa*. The sample is
1246 nonetheless too small to reliably decide whether the cranial scute splitting in large specimens
1247 may be treated as typical for *P. robusta* due to some specific developmental, structural or
1248 ecological susceptibility. The interpretation of this morphology as abnormality, part of a normal
1249 intraspecific variability, or a specific character is, therefore, impossible.

1250

1251 **Discussion**

1252 **Ontogeny**

1253 The shell of proterochersids changed during ontogeny in several ways. The most notable is the
1254 expansion of gular, extragular, and caudal processes (Figs 3, 5, 8–10, S7), and projections of
1255 cranial (Fig. 4) and caudal marginals (Fig. S5). In young specimens these elements were short
1256 and lack pronounced tips (e.g., Figs 4A, 5A, 8, 9 J–K, 10, S5BE, G), while in older specimens
1257 they were becoming proportionally larger. The nuchal notch formed by expansion of cranial
1258 marginals relative to cervical scute (Fig. 4). Furthermore, the depth and width of shell sulci
1259 increased with ontogenetic age (e.g., Figs S1B, L, N, O, S3, S4 A, C, E). This is linked to
1260 increase of sulci undulation and radial striation of scute areas (e.g., Fig. S8A–B, E–G). In some
1261 subadult and adult specimens, bow-shaped growth marks appeared on the scutes (e.g., Figs 6,
1262 S8A–F). As discussed above, a middorsal keel (e.g., Fig. S4) was apparently present in juveniles
1263 and reduced or lost in older specimens. A middorsal keel is also present in juveniles of at least
1264 some extant pleurodires (Ferreira, pers. comm. 2018) and cryptodires (e.g., Staurotypinae,
1265 Testudinidae, Emydidae, Platysternidae, Cheloniidae; Geoemydidae; Szczygielski, pers. obs.;
1266 Ascarrunz, pers. comm. 2018) but this feature is not documented well in the literature. The
1267 dorsal vertebrae were ankylosed in subadults and adults, and the axial skeleton mostly expanded
1268 at the points of rib head attachments (e.g. Fig. S1F–G). The neural canal changed its shape from
1269 vertically elongated to oval (Fig. S2).

1270

1271 **Sexual dimorphism**

1272 A wide array of sexually dimorphic characters is known in turtles (see Table S7 for examples).

1273 Many of these characters, unfortunately, are either unavailable for study in fossil material

1274 (cloacal position, hindlimb callosities) or impossible to check in currently collected

1275 *Proterochersis* spp. material due to its incompleteness (e.g., tail length, paw morphology) or

1276 damage and distortion (shape of the shell). Among the Triassic taxa, probable dimorphism was

1277 proposed for *Proganochelys quenstedti* in form of two morphotypes of hypoischium (Gaffney,

1278 1990).

1279 As noted above (see Results section), there is a very wide spectrum of sizes, within which the

1280 shells of *Proterochersis* spp. are ankylosed. It appears that all of the individuals possessed a

1281 ventral plastral concavity, and while it is possible that the dimorphism was expressed in varied

1282 depth or area of this concavity, the breakage and possible compaction of specimens prevent from

1283 using sensitive numerical methods, such as the Principal Component Analysis, to reliably check

1284 this. While size dimorphism may be present in *Proterochersis* spp., this difference in size does

1285 not explain the presence of ankylosis in even smaller specimens, such as ZPAL V.39/34.

1286 Similarly, the incompleteness, crushing, and possible compaction preclude utility of these

1287 methods to identify subtle dimorphisms in the carapace. The gular and extragular processes of

1288 the cranial plastral lobe and the caudal processes of the caudal plastral lobe, on the other hand,

1289 are relatively well-preserved and apparently not deformed in numerous specimens, and these

1290 regions of the shell are known to be dimorphic in some Testudines (Brophy, 2006; Pritchard,

1291 2008; Cadena, Jaramillo & Bloch, 2013; Leuteritz & Gantz, 2013; Sullivan & Joyce, 2017).

1292 The tubercles in the gular plastral region are usually larger in males of modern turtles, especially

1293 those with combat-based mating behaviors (Pritchard, 2008). This makes the variable gular

1294 region of the plastron of *Proterochersis* spp. potentially dimorphic. While initial observations

1295 revealed that there are two main post-juvenile morphotypes of the extragular projections

1296 independent from the size of the animal – one with the extragulars ventrally flat and roughly

1297 parallel to the cranial region of the humeral, and the second with the cranial tip of the extragulars

1298 turned ventrally, no clustering indicative of a dimorphism was found in our PCA and regression

1299   analyses (Fig. 8). It may be noted that the performed analyses was only focused on the extragular

1300   (and, in ventral view, gular) shape in separation from the rest of the plastron. For that reason it

1301   might have downplayed or failed to grasp some of the morphological characteristics of that

1302   region, such as the angle between the extragular projection and the plane of the rest of the cranial

1303   plastral lobe. Exclusion of the humeral scute area, caudal to the gulars and extragulars, was

1304   necessary at this time, because many of the studied specimens lack most or all of that part,

1305   rendering reliable positioning of the landmarks impossible. New, more complete specimens and,

1306   possibly, utilization of 3D morphometrics may, however, yield other results and should be

1307   attempted in the future.

1308   The variability of the caudal processes (Figs 9–10) is seemingly much larger in *Proterochersis*

1309   spp. than the variability in the gular region. Typically, the depth, width, and shape of anal notch

1310   is correlated with sex (Brophy, 2006; Pritchard, 2008; Cadena, Jaramillo & Bloch, 2013;

1311   Leuteritz & Gantz, 2013; Sullivan & Joyce, 2017). Usually, males have deeper notches than

1312   females, to facilitate movement of cloaca-supporting tail during copulation (Brophy, 2006;

1313   Cadena, Jaramillo & Bloch, 2013; Sullivan & Joyce, 2017), but there are taxa in which females

1314   have deeper notches, possibly to facilitate oviposition (Leuteritz & Gantz, 2013). Proterochersids

1315   lack typical anal notch, because their xiphiplastra did not reach the caudal edge of the plastron,

1316   and three caudal plastral ossifications (possibly homologous to hypoischium, but more data are

1317   needed to unambiguously prove or refute this homology) were instead sutured behind them

1318   (Szczygielski & Sulej, 2019), but functionally the space between the caudal processes may be

1319   compared to anal notch of pleurodires and some cryptodires. The structure of cloaca and penis is,

1320   obviously, unknown for the Triassic turtles, but it may be hypothesized that the notch between

1321   the caudal processes would bring them analogous benefits. Furthermore, the hypoischium of

1322   Triassic turtles, which was located just caudal to the pelvis and plastron, usually had two

1323   fingerlike caudal processes (Gaffney, 1990; Sterli, de la Fuente & Rougier, 2007; Li et al., 2008;

1324   Szczygielski & Sulej, 2019). This structure at least in some Triassic testudinates was dimorphic

1325   and likely played a role during copulation (Gaffney, 1990; Szczygielski & Sulej, 2019).

1326   Although no clear-cut clusters were recovered, the shape analysis shows that the specimens with

1327   long, spiky, widely spread caudal processes, such as SMNS 12777, ZPAL V.39/48, or ZPAL

1328   V.39/49, do not mix with those with short, rounded caudal processes, such as CSMM uncat.,

1329   SMNS 17561, or ZPAL V.39/69 (consistently with long caudal process of ischium of ZPAL

1330   V.39/69, which blocks the space between the caudal processes and would likely get in the way of

1331   male tail), which may hint some (possibly sexual-related) selection towards separation of the

1332   caudal processes' shape in adults. This picture is, however, distorted by odd specimens – ZPAL

1333   V.39/68 (long caudal processes, but very close together) and ZPALV.39/71 (long, widely spread

1334   caudal processes, but the space between them is at least partially blocked by ischium). It must be

1335   kept in mind that this is the worst preserved specimen in the tested group and its edges are worn,

1336   so the exact extent of its caudal ischial plate and exact length of the caudal processes may be

1337   misrepresented. Unfortunately, ZPAL V.39/69 is too fragmentary to include it in the shape

1338   analysis.

1339

Conclusions

1341   *Proterochersis robusta* and *P. porebensis* are found to be very similar to each other in most

1342   aspects of their anatomy and variability, although they exhibit some apparently consistent

1343   differentiating characters that support their specific identity – most notably, the shape of the

1344   caudal notch (semicircular in *P. robusta* versus triangular in *P. porebensis*; Szczygielski & Sulej,

1345   2016) and the position of the costoperipheral suture in the bridge region (around the middle of

1346   the supramarginals in *P. robusta* versus at the level of marginosupramarginal sulcus in *P.*

1347   *porebensis*; Szczygielski & Sulej, 2019). Here, we also add the maximal size and the tempo of

1348   growth (larger in *P. porebensis* than in *P. robusta*) to this list. Some other characters described

1349   here (e.g., tendency for vertebral scute splitting in *P. robusta*, more exaggerated morphology of

1350   the extragulars in *P. porebensis*) may also prove taxonomically diagnostic, but more specimens

1351   must be recovered and studied before this is confirmed. Szczygielski and Sulej (2016) also noted

1352   the shape of the anterior marginals (serrated in *P. robusta* versus straight in *P. porebensis*) and

1353   the profile of the shell (higher in *P. robusta* than in *P. porebensis*) as diagnostic for the species.

1354   These characters remain in force, but must be treated with adequate awareness. The anterior edge

1355   of the carapace is preserved intact only in several specimens, so variability in that regard cannot

1356   be refuted, especially in light of the significant variability of marginals described in this work.

1357   The exact geometry of the shell, on the other hand, is difficult to establish in *P. porebensis* due to

1358   crushing or incompleteness of all available specimens. Future discoveries of new material will

1359   likely validate or refute the status of these characters.

The observations of shell variation in Proterochersidae reveals, as could be anticipated, that these oldest true turtles being the sister group to all other known testudinatans (Szczygielski & Sulej, 2016, 2019), exhibited numerous progressive characters already resembling derived turtles (e.g., patterns of scute growth, intervertebral position of dorsal ribs), but some either plesiomorphic for Testudinata (radial striation of carapacial scutes) or difficult to assess (deep troughs surrounding laterally the middorsal keel in young individuals, seemingly common medial splitting of vertebral scutes).The presence of growth marks and shell abnormalities comparable to those occurring in modern turtles suggest that the scute system of *Proterochersis* spp. was already controlled by similar developmental mechanism as in crown group taxa. The cranialmost and caudalmost regions of the plastron are hypothesized to be sexually dimorphic in *Proterochersis* spp. No clustering was found on the PCA analysis of gular and extragular tubercles, indicating a population variability without a clear cause (Fig. 8). Nonetheless, some indistinct separation can be observed between the specimens with spiky and rounded caudal processes and implies that they may represent a form of sexual dimorphism of *Proterochersis* spp.(Fig. 10A–C). The variability in that region is not explained by ontogeny alone. Therefore, it seems that the sexual dimorphism in the anal region of the plastron, which can be observed in some species of extant turtles (most notably pleurodires, but also some cryptodires; see, e.g., Brophy, 2006; Pritchard, 2008; Cadena, Jaramillo & Bloch, 2013; Leuteritz & Gantz, 2013; Sullivan & Joyce, 2017) might have been present also in the beginning of their evolution, in the oldest true turtles, around 215 million years ago. Confirmation or refusal of this hypothesis, however, requires a larger sample size and for now this observation must be treated as a pointer for future research rather than definitive statement.

Acknowledgements

We thank Rainer Schoch for access to SMNS collection, Carl Schweizer for granting access to CSMM collection, Łucja Fostowicz-Frelik for the macrophotographs of ZPAL V.39/381 and ZPAL V.39/384, Marco Marzola for 3D models of ZPAL V.39/34 and ZPAL V.39/48, Tomasz Sulej for discussion, and Piotr Bajdek for additional preparation work, as well as Jérémy Anquetin (the Editor), Eduardo Ascarrunz, Gabriel Ferreira, and Julien Claude (the Reviewers),

1389   and the Production Office for their very helpful comments and work needed to process and

1390   improve this manuscript.

1391

References

1393   Alibardi L. 2005. Proliferation in the epidermis of chelonians and growth of the horny scutes.

1394   *Journal of Morphology* 265:52–69. DOI: 10.1002/jmor.10337.

1395   Anquetin J., Claude J. 2008. Reassessment of the oldest British turtle: *Protochelys* from the

1396   Middle Jurassic Stonesfield Slate of Stonesfield, Oxfordshire, UK. *Geodiversitas* 30:331–

1397   344.

1398   Anquetin J., Joyce WG. 2014. A reassessment of the Late Jurassic turtle *Eurysternum wagleri*

1399   (Eucryptodira, Eurysternidae). *Journal of Vertebrate Paleontology* 34:1317–1328. DOI:

1400   10.1080/02724634.2014.880449.

1401   Anquetin J., Püntener C., Billon-Bruyat J-P. 2014. A taxonomic review of the Late Jurassic

1402   eucryptodiran turtles from the Jura Mountains (Switzerland and France). *PeerJ* 2:e369.

1403   DOI: doi: 10.7717/peerj.369.

1404   Anquetin J., Püntener C., Joyce WG. 2017. A review of the fossil record of turtles of the clade

1405   Thalassochelydia. *Bulletin of the Peabody Museum of Natural History* 58:317–369. DOI:

1406   10.3374/014.056.0203.

1407   Baur G. 1887. Ueber den Ursprung der Extremitäten der Ichthyopterygia. *Berichte über*

1408   *Versammlungen des Oberrheinischen Vereines* 20:17–20.

1409   Berry JF., Shine R. 1980. Sexual size dimorphism and sexual selection in turtles (order

1410   Testudines). *Oecologia* 44:185–191.

1411   Bookstein FL. 1997. *Morphometric tools for landmark data: Geometry and biology*. Cambridge

1412   University Press.

1413   Broin F de. 1994. Données préliminaires sur les chéloniens du Tithonien inférieur des calcaires

1414   lithographiques de Cajuers (Var, France). *Geobios* 16:167–175.

1415   de Broin F., Ingavat R., Janvier P., Sattayarak N. 1982. Triassic turtle remains from northeastern
1416   Thailand. *Journal of Vertebrate Paleontology* 2:41–46.

1417   Brophy TR. 2006. Allometry and sexual dimorphism in the snail-eating turtle *Malayemys*
1418   *macrocephala* from the Chao Phraya River Basin of central Thailand. *Chelonian*
1419   *Conservation and Biology* 5:159–165. DOI: 10.2744/1071-
1420   8443(2006)5[159:AASDIT]2.0.CO;2.

1421   Burke AC. 1989. Development of the turtle carapace: Implications for the evolution of a novel
1422   bauplan. *Journal of Morphology* 199:363–378. DOI: 10.1002/jmor.1051990310.

1423   Burke AC., Nowicki JN. 2003. A new view of patterning domains in the vertebrate mesoderm.
1424   *Developmental Cell* 4:159–165. DOI: 10.1016/S1534-5807(03)00033-9.

1425   Cadena EA., Jaramillo CA., Bloch JI. 2013. New material of the platychelyid turtle *Notoemys*
1426   *zapatocaensis* from the Early Cretaceous of Colombia; Implications for understanding
1427   Pleurodira evolution. In: Brinkman DB, Holroyd PA, Gardner JD eds. *Morphology and*
1428   *Evolution of Turtles*. Dordrecht: Springer Science+Business Media, 105–120.

1429   Cherepanov GO. 1989. New morphogenetic data on the turtle shell: discusion on the origin of
1430   the horny and bony parts. *Studia Geologica Salmanticensia* 3:9–24.

1431   Cherepanov GO. 2006. Ontogenesis and evolution of horny parts of the turtle shell. *Fossil Turtle*
1432   *Research* 1:19–33.

1433   Cherepanov GO. 2014. Patterns of scute development in turtle shell: Symmetry and asymmetry.
1434   *Paleontological Journal* 48:1275–1283. DOI: 10.1134/S0031030114120028.

1435   Cherepanov GO. 2015. Scute's polymorphism as a source of evolutionary development of the
1436   turtle shell. *Paleontological Journal* 49:1–10.

1437   Cherepanov GO. 2016. Nature of the turtle shell: Morphogenetic causes of bone variability and
1438   its evolutionary implication. *Paleontological Journal* 50:1641–1648. DOI:
1439   10.1134/S0031030116140033.

1440   Cignoni P., Callieri M., Corsini M., Dellepiane M., Ganovelli F., Ranzuglia G. 2008. MeshLab:
1441   An open-source mesh processing tool. In: *Sixth Eurographics Italian Chapter Conference*.
1442   129–136. DOI: 10.2312/LocalChapterEvents/ItalChap/ItalianChapConf2008/129-136.

1443   Coker RE. 1905. Orthogenetic variation? *Science* 22:873–875.

1444   Coker RE. 1910. Diversity in the scutes of Chelonia. *Journal of Morphology* 21:1–75.

1445   Farke CM., Distler C. 2015. Ontogeny and abnormalities of the tortoise carapace: A computer
1446   tomography and dissection study. *Salamandra* 51:231–244.

1447   Fraas E. 1913. *Proterochersis*, eine pleurodire Schildkröte aus dem Keuper. *Jahreshefte des*
1448   *Vereins für Vaterlandische Naturkunde in Württemberg* 69:13–30.

1449   Frye FL. 1994. Diagnosis and surgical treatment of reptilian neoplasma with a compilation of
1450   cases 1966–1993. *In Vivo* 8:885–892.

1451   Gadow H. 1905. Orthogenetic variation. *Science* 22:637–640.

1452   Gaffney ES. 1990. The comparative osteology of the Triassic turtle *Proganochelys*. *Bulletin of*
1453   *the American Museum of Natural History* 194:1–263.

1454   Gilbert SF., Loredo GA., Brukman A., Burke AC. 2001. Morphogenesis of the turtle shell: The
1455   development of a novel structure in tetrapod evolution. *Evolution & Development* 3:47–58.
1456   DOI: 10.1046/j.1525-142X.2001.003002047.x.

1457   Gmelin SG. 1774. *Reise durch Russland zur Untersuchung der drey Natur-Reiche. Dritter Theil.*
1458   *Reise durch das nordliche Persien, in den Jahren 1770, 1771, bis April 1772.* Saint
1459   Petersburg: Kayserliche Akademie der Wissenschaften.

1460   Grant C. 1936a. The "midventral keel" in Testudinata. *Proceedings of the Indiana Academy of*
1461   *Science*:246–252. DOI: 10.1007/s10641-007-9325-3.

1462   Grant C. 1936b. Orthogenetic variation. *Proceedings of the Indiana Academy of Science* 46:240–
1463   245.

1464   Hutchison JH., Bramble DM. 1981. Homology of the plastral scales of the Kinosternidae and

1465   related turtles. *Herpetologica* 37:73–85.

1466   Jansen M., Klein N. 2014. A juvenile turtle (Testudines, Eucryptodira) from the Upper Jurassic
1467   of Langenberg Quarry, Oker, Northern Germany. *Palaeontology* 57:743–756. DOI:
1468   10.1111/pala.12085.

1469   Joyce WG., Lucas SG., Scheyer TM., Heckert AB., Hunt AP. 2009. A thin-shelled reptile from
1470   the Late Triassic of North America and the origin of the turtle shell. *Proceedings of the*
1471   *Royal Society of London B: Biological Sciences* 276:507–513. DOI:
1472   10.1098/rspb.2008.1196.

1473   Karl H-V., Tichy G. 2000. *Murrhardtia staeschei* n. gen. n. sp. – eine neue Schildkröte aus der
1474   Oberen Trias von Süddeutschland. *Joannea Geologie und Paläontologie* 2:57–72.

1475   Klingenberg CP. 1996. Multivariate allometry. In: Marcus LF, Corti M, Loy A, Naylor GJP,
1476   Slice DE eds. *Advances in Morphometrics*. Boston: Springer, 23–49.

1477   Klingenberg CP. 2009. Morphometric integration and modularity in configurations of landmarks:
1478   Tools for evaluating a priori hypotheses. *Evolution and Development* 11:405–421. DOI:
1479   10.1111/j.1525-142X.2009.00347.x.

1480   Klingenberg CP. 2011. MorphoJ: An integrated software package for geometric morphometrics.
1481   *Molecular Ecology Resources* 11:353–357. DOI: 10.1111/j.1755-0998.2010.02924.x.

1482   Kordikova EG. 2002. Heterochrony in the evolution of the shell of Chelonia. Part 1:
1483   Terminology, Cheloniidae, Dermochelyidae, Trionychidae, Cyclanorbidae and
1484   Carettochelyidae. *Neues Jahrbuch für Geologie und Paläontologie - Abhandlungen*
1485   226:343–417.

1486   Leuteritz TEJ., Gantz DT. 2013. Sexual Dimorphism in Radiated Tortoises (*Astrochelys*
1487   *radiata*). *Chelonian Research Monographs* 6:105–112. DOI: 10.3854/crm.6.a18p105.

1488   Li C., Wu X-C., Rieppel OC., Wang L-T., Zhao L-J. 2008. An ancestral turtle from the Late
1489   Triassic of southwestern China. *Nature* 456:497–501. DOI: 10.1038/nature07533.

1490   Lichtig AJ., Lucas S. 2017. Sutures of the shell of the Late Cretaceous-Paleocene baenid turtle

1491   *Denazinemys. Neues Jahrbuch für Geologie und Paläontologie - Abhandlungen* 283:1–8.
1492   DOI: 10.1127/njgpa/2017/0622.

1493   Linnaeus C. 1758. *Systema naturae per regna tria naturae, secundum classes, ordines, genera,*
1494   *species, cum characteribus, differentiis, synonymis, locis. T. I*. Holmiae: Laurentii Salvii.

1495   Lucas SG., Heckert AB., Hunt AP. 2000. Probable turtle from the Upper Triassic of east-central
1496   New Mexico. *Neues Jahrbuch für Geologie und Paläontologie - Monatshefte* 5:287–300.

1497   Lynn WG. 1937. Variation in scutes and plates in the box-turtle, *Terrapene carolina. The*
1498   *American Naturalist* 71:421–427.

1499   Lynn WG., Ullrich MC. 1950. Experimental production of shell abnormalities in turtles. *Copeia*
1500   1950:253–262.

1501   McEwan B. 1982. Bone anomalies in the shell of *Gopherus polyphemus. Florida Scientist*
1502   45:189–195.

1503   McKnight DT., Ligon DB. 2014. Shell and pattern abnormalities in a population of western
1504   chicken turtles (*Deirochelys reticularia miaria*). *Herpetology Notes* 7:89–91.

1505   Młynarski M. 1956. Studies on the morphology of the shell of recent and fossil tortoises. I-II.
1506   *Acta Zoologica Cracoviensia* 1:1–19.

1507   Moustakas-Verho JE., Cebra-Thomas J., Gilbert SF. 2017. Patterning of the turtle shell. *Current*
1508   *Opinion in Genetics & Development* 45:124–131. DOI: 10.1016/j.gde.2017.03.016.

1509   Moustakas-Verho JE., Cherepanov GO. 2015. The integumental appendages of the turtle shell:
1510   An evo-devo perspective. *Journal of Experimental Zoology Part B: Molecular and*
1511   *Developmental Evolution* 324:221–229. DOI: 10.1002/jez.b.22619.

1512   Moustakas-Verho JE., Zimm R., Cebra-Thomas JA., Lempiäinen NK., Kallonen A., Mitchell
1513   KL., Hämäläinen K., Salazar-Ciudad I., Jernvall J., Gilbert SF. 2014. The origin and loss of
1514   periodic patterning in the turtle shell. *Development* 141:3033–3039. DOI:
1515   10.1242/dev.109041.

1516   Newman HH. 1906a. The significance of scute and plate "abnormalities" in Chelonia. A

1517   contribution to the evolutionary history of the chelonian carapace and plastron. Part II.

1518   *Biological Bulletin* 10:99–114.

1519   Newman HH. 1906b. The significance of scute and plate "abnormalities" in Chelonia. A

1520   contribution to the evolutionary history of the chelonian carapace and plastron. Part I.

1521   *Biological Bulletin* 10:68–98.

1522   Niedźwiedzki G., Brusatte SL., Sulej T., Butler RJ. 2014. Basal dinosauriform and theropod

1523   dinosaurs from the mid-late Norian (Late Triassic) of Poland: Implications for Triassic

1524   dinosaur evolution and distribution. *Palaeontology* 57:1121–1142. DOI:

1525   10.1111/pala.12107.

1526   Nowicki JN., Burke AC. 2000. *Hox* genes and morphological identity: Axial versus lateral

1527   patterning in the vertebrate mesoderm. *Development* 127:4265–4275.

1528   Özdemir B., Türkozan O. 2006. Carapacial scute variation in green turtle, *Chelonia mydas*

1529   hatchlings in Northern Cyprus. *Turkish Journal of Zoology* 30:141–146.

1530   Parker GH. 1901. Correlated abnormalities in the scutes and bony plates of the carapace of the

1531   sculptured tortoise. *The American Naturalist* 35:17–24. DOI: 10.1525/tph.2001.23.2.29.

1532   Pritchard PCH. 2008. Evolution and structure of the turtle shell. In: Wyneken J, Godfrey MH,

1533   Bels V eds. *Biology of Turtles*. Boca Raton, London & New York: CRC Press, 46–83.

1534   Rice R., Kallonen A., Cebra-Thomas JA., Gilbert SF. 2016. Development of the turtle plastron,

1535   the order-defining skeletal structure. *Proceedings of the National Academy of Sciences of*

1536   *the United States of America* 113:5317–5322. DOI: 10.1073/pnas.1600958113.

1537   Rohlf FJ. 2015. The tps series of software. *Hystrix* 26:1–4. DOI: 10.4404/hystrix-26.1-11264.

1538   Rothschild BM., Schultze H-P., Pellegrini R. 2013. Osseous and other hard tissue pathologies in

1539   turtles and abnormalities of mineral deposition. In: Brinkman DB, Holroyd PA, Gardner JD

1540   eds. *Morphology and Evolution of Turtles*. Dordrecht: Springer Science+Business Media,

1541   501–534.

1542   Schoch RR., Sues H-D. 2015. A Middle Triassic stem-turtle and the evolution of the turtle body

1543   plan. *Nature* 523:584–587. DOI: 10.1038/nature14472.

1544   Schoch RR., Sues H-D. 2017. Osteology of the Middle Triassic stem-turtle *Pappochelys rosinae*
1545   and the early evolution of the turtle skeleton. *Journal of Systematic Palaeontology*:1–39.
1546   DOI: 10.1080/14772019.2017.1354936.

1547   Shearman RM., Burke AC. 2009. The lateral somitic frontier in ontogeny and phylogeny.
1548   *Journal of Experimental Zoology Part B: Molecular and Developmental Evolution*
1549   312:603–612. DOI: 10.1002/jez.b.21246.The.

1550   Sterli J., de la Fuente MS., Rougier GW. 2007. Anatomy and relationships of *Palaeochersis*
1551   *talampayensis*, a Late Triassic turtle from Argentina. *Palaeontographica Abteilung A*
1552   281:1–61.

1553   Sulej T., Niedźwiedzki G., Bronowicz R. 2012. A new Late Triassic vertebrate fauna from
1554   Poland with turtles, aetosaurs, and coelophysoid dinosaurs. *Journal of Vertebrate*
1555   *Paleontology* 32:1033–1041. DOI: 10.1080/02724634.2012.694384.

1556   Sullivan PM., Joyce WG. 2017. The shell and pelvic anatomy of the Late Jurassic turtle
1557   *Platychelys oberndorferi* based on material from Solothurn, Switzerland. *Swiss Journal of*
1558   *Palaeontology* 136:323–343.

1559   Szczygielski T. 2017. Homeotic shift at the dawn of the turtle evolution. *Royal Society Open*
1560   *Science* 4:160933. DOI: http://dx.doi.org/10.1098/rsos.160933.

1561   Szczygielski T., Sulej T. 2016. Revision of the Triassic European turtles *Proterochersis* and
1562   *Murrhardtia* (Reptilia, Testudinata, Proterochersidae), with the description of new taxa
1563   from Poland and Germany. *Zoological Journal of the Linnean Society* 177:395–427. DOI:
1564   10.1111/zoj.12374.

1565   Szczygielski T., Sulej T. 2019. The early composition and evolution of the turtle shell (Reptilia,
1566   Testudinata). *Palaeontology*.

1567   Szulc J., Racki G., Jewuła K., Środoń J. 2015. How many Upper Triassic bone-bearing levels are
1568   there in Upper Silesia (Southern Poland)? A critical overview of stratigraphy and facies.
1569   *Annales Societatis Geologorum Poloniae* 85:587–626. DOI: 10.14241/asgp.2015.037.

1570   Velo-Antón G., Becker CG., Cordero-Rivera A. 2011. Turtle carapace anomalies: The roles of

1571   genetic diversity and environment. *PLoS ONE* 6:e18714. DOI:

1572   10.1371/journal.pone.0018714.

1573   Wibbels T., Owens DW., Rostal DC. 1991. Soft plastra of adult male sea turtles: An apparent

1574   secondary sexual characteristic. *Herpetological Review* 22:47–49.

1575   Wu C. 2011.VisualSFM: A visual structure from motion system

1576   Wyneken J. 2001. *The anatomy of sea turtles*. U.S. Department of Commerce NOAA Technical

1577   Memorandum NMFS-SEFSC-470.

1578   Yntema CL. 1970. Extirpation experiments on embryonic rudiments of the carapace of *Chelydra*

1579   *serpentina*. *Journal of Morphology* 132:235–244. DOI: 10.1002/jmor.1051320209.

1580   Zangerl R. 1939. The homology of the shell elemests in turtles. *Journal of Morphology* 65:383–

1581   409.

1582   Zangerl R. 1969. The turtle shell. In: Gans C ed. *Biology of the Reptilia*. London & New York:

1583   Academic Press, 311–339.

1584   Zangerl R., Johnson RG. 1957. The nature of shield abnormalities in the turtle shell. *Fieldiana*

1585   *Geology* 10:341–362. DOI: 10.1017/CBO9781107415324.004.

1586   Zatoń M., Niedźwiedzki G., Marynowski L., Benzerara K., Pott C., Cosmidis J., Krzykawski T.,

1587   Filipiak P. 2015. Coprolites of Late Triassic carnivorous vertebrates from Poland: An

1588   integrative approach. *Palaeogeography, Palaeoclimatology, Palaeoecology* 430:21–46.

1589   DOI: 10.1016/j.palaeo.2015.04.009.

1590   Zelditch ML., Swiderski DL., Sheets HD., Fink WL. 2004. *Geometric morphometrics for*

1591   *biologists: a primer*. New York, London: Academic Press.

1592

Figure 1

Nomenclature of turtle scutes shown on the reconstruction of the shell of *Proterochersis robusta* in (A) dorsal, (B) lateral left, and (C) ventral view, and the legend of color and pattern codes used.
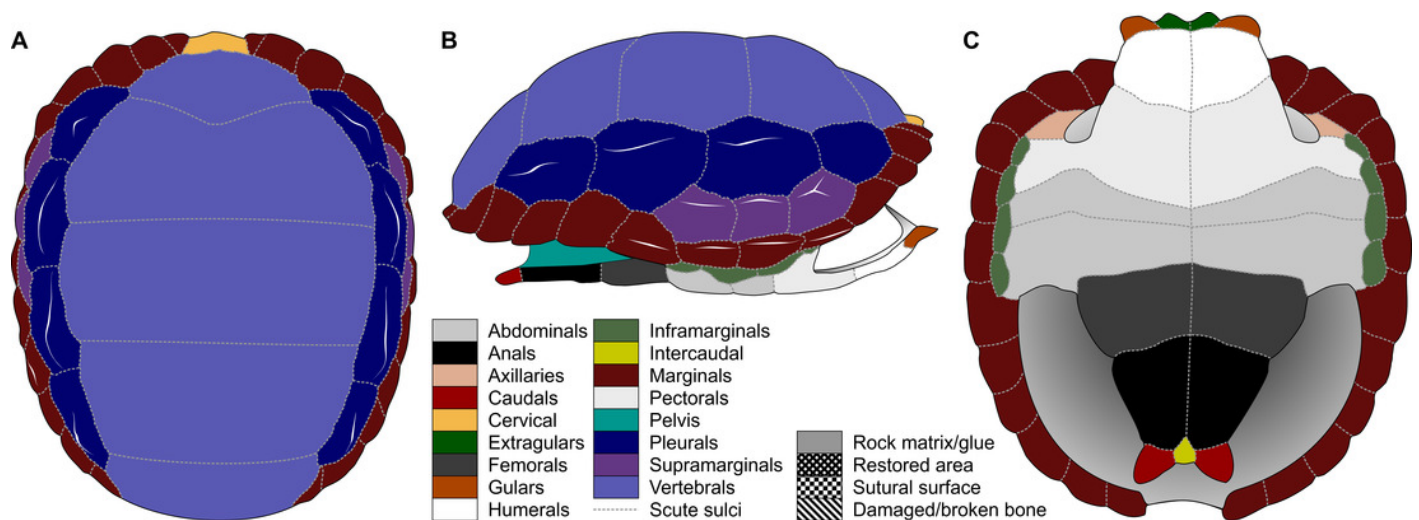
Figure 2

External carapace morphology of *Proterochersis robusta*.

(A, B) CSMM uncat. in (A) dorsal and (B) lateral right view; (C) SMNS 16442, carapace in dorsal view; (D, E) SMNS 16603 in (D) dorsal and (E) lateral right view; (F, G) SMNS 17561 in (F) dorsal and (G) lateral left (mirrored) view; (H) SMNS 17755a in dorsal view; (I, J) 17930 in (I) dorsal and (J) lateral right view. (K) SMNS 18440 in lateral left (mirrored) view. Restored area not shown for SMNS 17561 (F, G) due to difficulties in evaluation. Minor damage and restorations not shown for clarity.
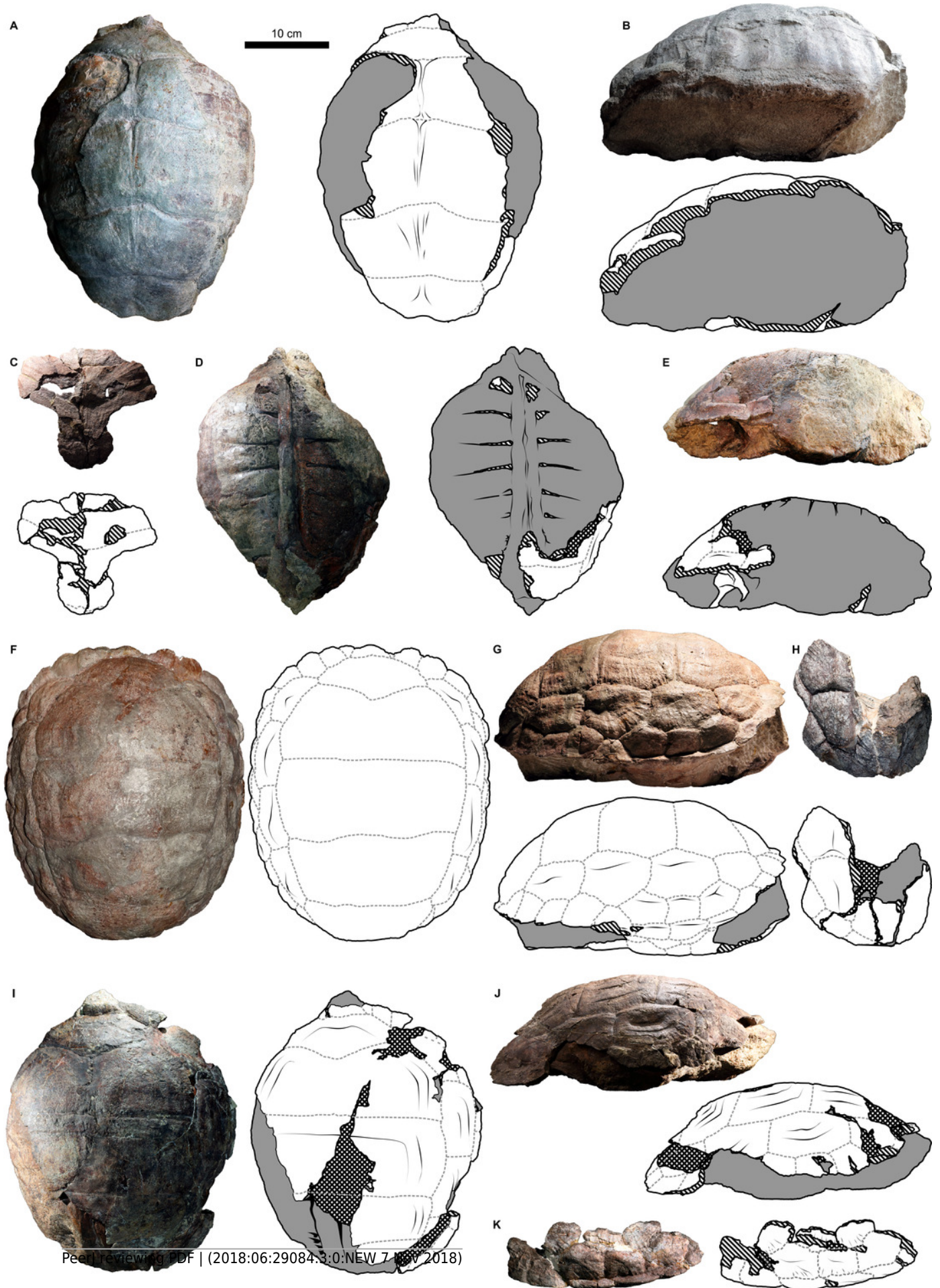
Figure 3

External plastron morphology of *Proterochersis robusta*.

(A) CSMM uncat. in ventral view; (B) SMNS 11396, plastron in ventral view; (C) SMNS 12777 in ventral view; (D) SMNS 16442, plastron in ventral view; (E) SMNS 16603, plastron in ventral view; (F) SMNS 17561 in ventral view; (G) SMNS 17755, plastron in ventral view; (H) SMNS 18440 in ventral view; (I) SMNS 50917 in ventral view; (J) SMNS 56606 in ventral view. Scute sulci are represented by dashed grey lines. Restored area not shown for SMNS 17561 (F) due to difficulties in evaluation. Minor damage and restorations not shown for clarity.
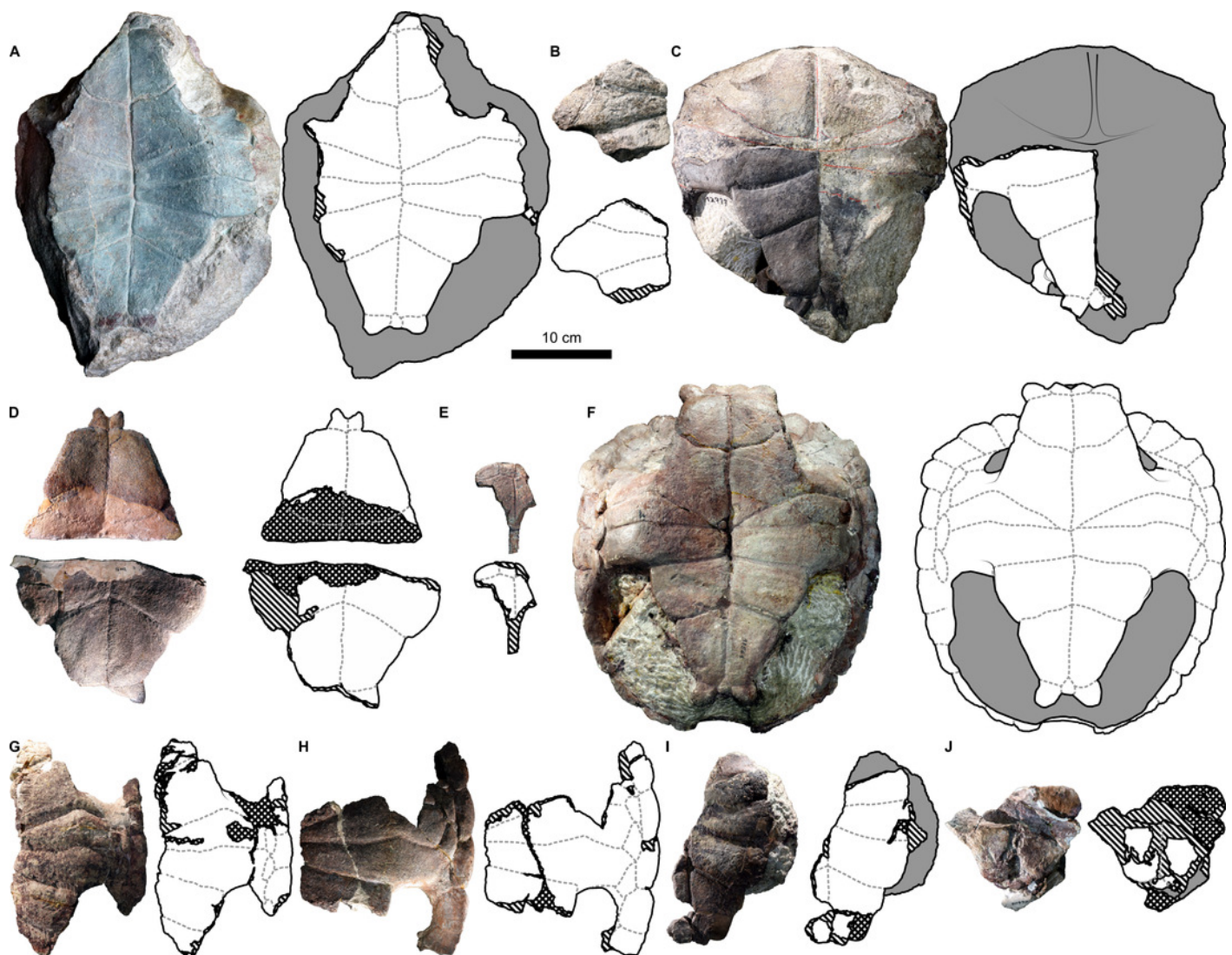
Figure 4

External carapace morphology of *Proterochersis porebensis*.

(A, B) ZPAL V.39/34 in (A) dorsal and (B) lateral left (mirrored) view; (C, D) ZPAL V.39/48, (C) carapace in dorsal and (D) lateral right view; (E, F) ZPAL V.39/49, (E) carapace in dorsal and (F) lateral right view; (G, H) ZPAL V.39/72 in (G) dorsal and (H) lateral left (mirrored) view. Minor damage and restorations not shown for clarity.

10 cm
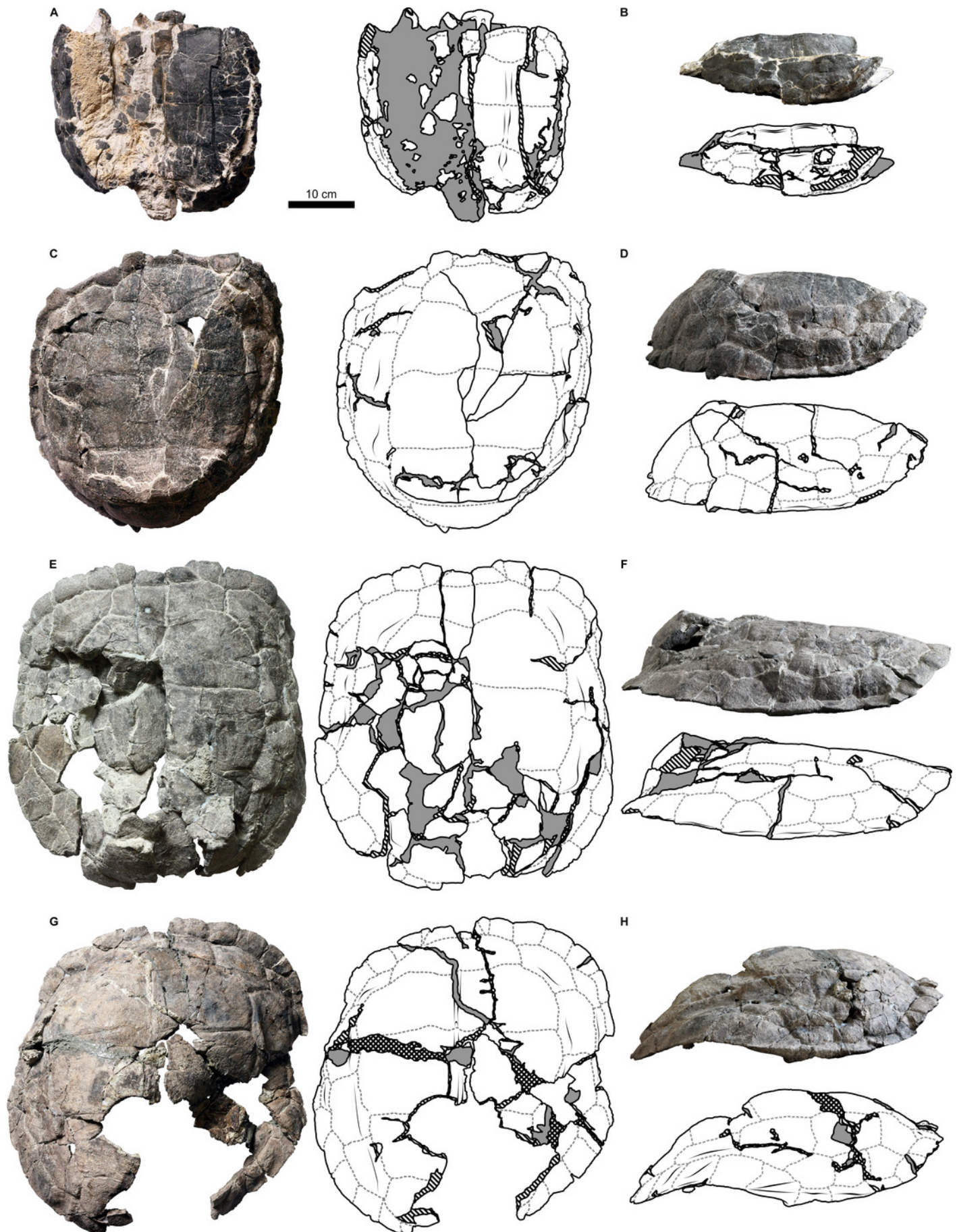
Figure 5

External plastron morphology of *Proterochersis porebensis*.

(A) ZPAL V.39/34 in ventral view; (B) ZPAL V.39/48 in ventral view; (C) ZPAL V.39/49 in ventral view. Minor damage and restorations not shown for clarity.
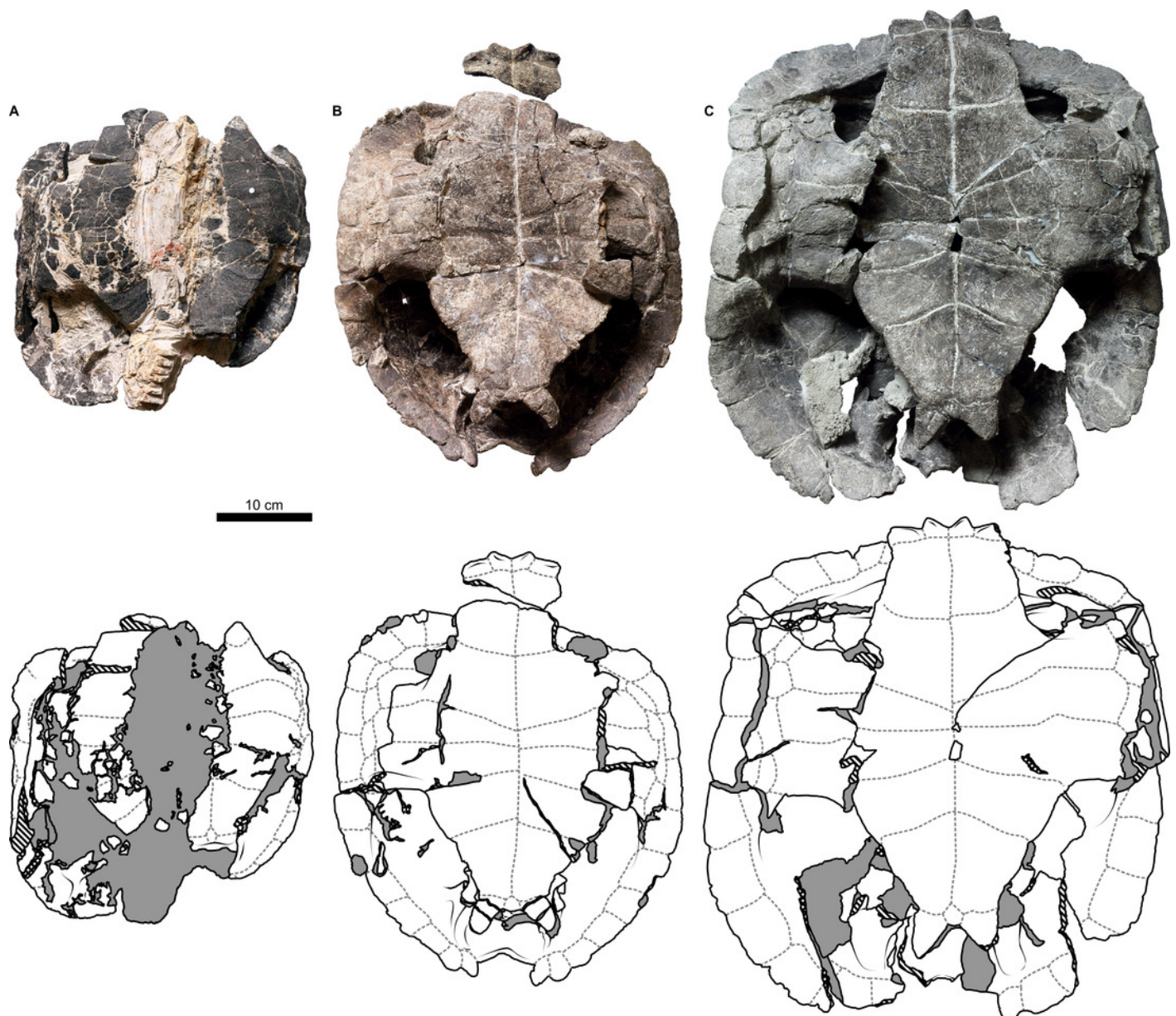
Figure 6

Proterochersis robusta, SMNS 17930, carapace in (A) lateral right, (B) laterodorsoanterior, and (C) dorsoanterior view.

Note pronounced growth marks.

Note: Auto Gamma Correction was used for the image. This only affects the reviewing manuscript. See original source image if needed for review.
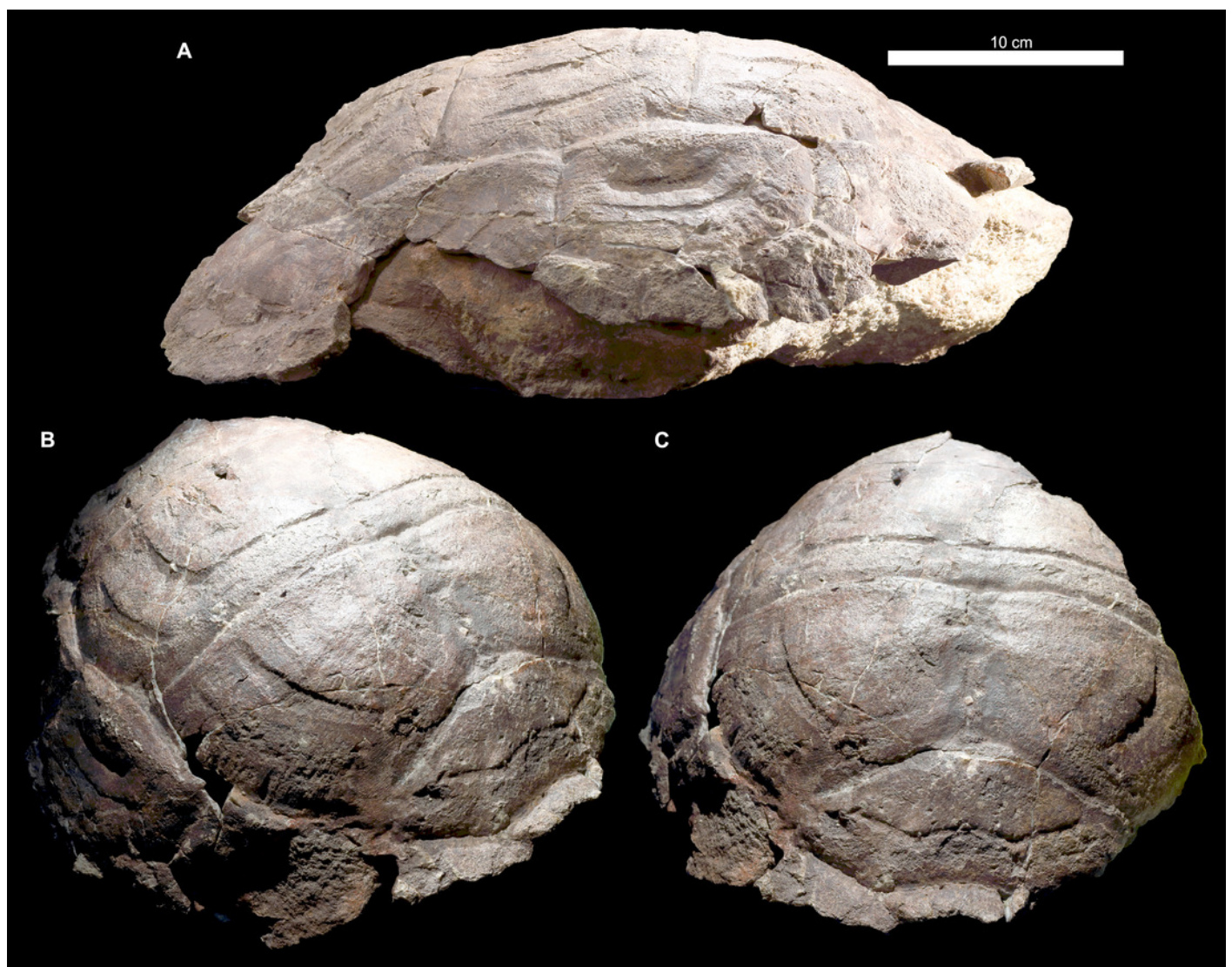
Figure 7

Proterochersis porebensis, ZPAL V.39/385, anterior plastral lobe with supernumerary scutes (*) in (A) visceral and (B) external view.
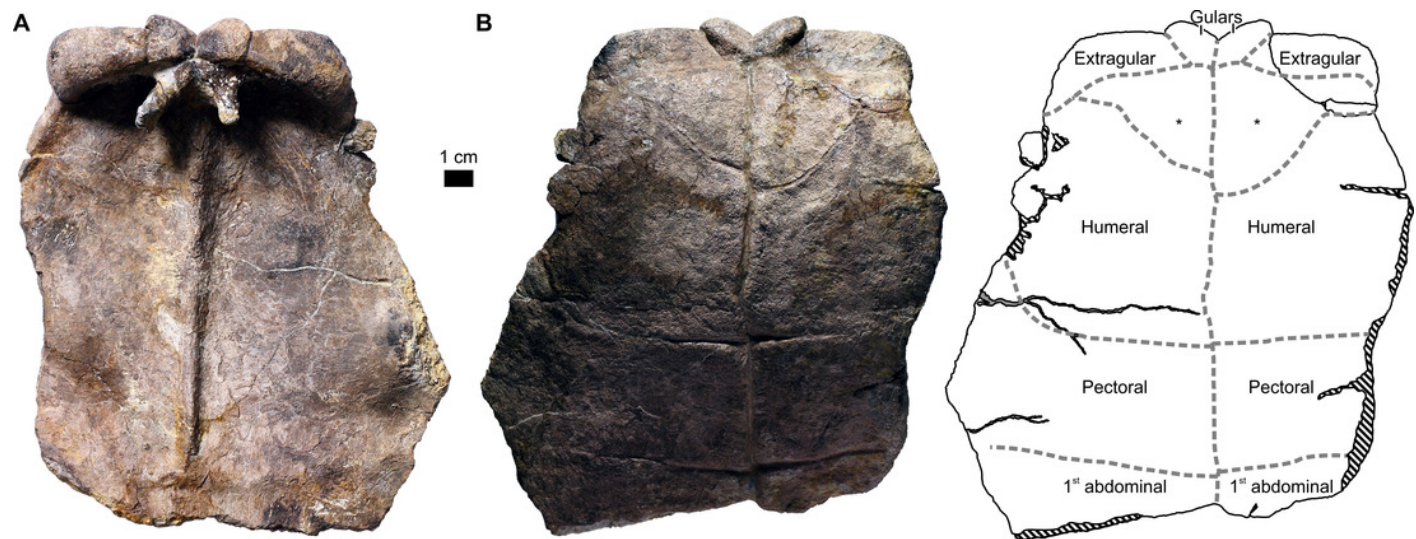
Figure 8

Results of the Principal Component Analysis of the gular plastral region in (A, B) ventral view and (C–F) vertical cross-section of extragulars.

The main shape changes for each PC are represented by wireframes, black wireframe is the average shape, while the red line represent shape changes connected to adequate PCs. *Proterochersis robusta* is represented by stars, *P. porebensis* by dots. Representations of scute shapes not to scale.

A

Principal component 2

- V.39/34
- V.39/388
- V.39/385
- V.39/387
- V.39/48
- V.39/379
- V.39/420
- V.39/49
- V.39/187
- SMNS 17561 ★
- V.39/333

Principal component 1

B

Principal component 3

- V.39/34
- V.39/187
- V.39/333
- SMNS 17561 ★
- V.39/387
- V.39/388
- V.39/385
- V.39/48
- V.39/379
- V.39/49
- V.39/420

Principal component 1

C

Principal component 2

- V.39/385
- V.39/49
- V.39/48
- V.39/333
- V.39/388
- V.39/420
- V.39/387
- V.39/379
- V.39/34
- V.39/187

Principal component 1

D

Principal component 3

- V.39/379
- V.39/49
- V.39/388
- V.39/420
- V.39/187
- V.39/385
- V.39/34
- V.39/333
- V.39/387
- V.39/48

Principal component 1

E

Regression score

- V.39/420
- V.39/187
- V.39/333
- SMNS 17561 ★
- V.39/385
- V.39/49
- V.39/388
- V.39/379
- V.39/48
- V.39/387
- V.39/34

Log Centroid size

F

Regression score

- V.39/333
- V.39/388
- V.39/48
- V.39/49
- V.39/385
- V.39/187
- V.39/387
- V.39/379
- V.39/34
- V.39/420

Log Centroid size

Figure 9

Variability of caudal region of plastron of (A–C) *Proterochersis robusta* and (D–T) *P. porebensis*.

(A) CSMM uncat.; (B) SMNS 12777; (C) SMNS 17561; (D) ZPAL V.39/49; (E) ZPAL V.39/71; (F) ZPAL V.39/69; (G) ZPAL V.39/48; (H) ZPAL V.39/68; (I) ZPAL V.39/70; (J) ZPAL V.39/66; (K) ZPAL V.39/34; (L–N) ZPAL V.39/56, left caudal process in (L) dorsal, (M) ventral, and (N) lateral view; (O–Q) ZPAL V.39/199, left caudal process in (O) dorsal, (P) ventral, and (Q) lateral view; (R–T) ZPAL V.39/200, (?)left caudal process in (R) dorsal, (S) ventral, and (T) lateral view. A–K in ventral view, in the same scale, ordered roughly by decreasing size. L–T in the same scale.
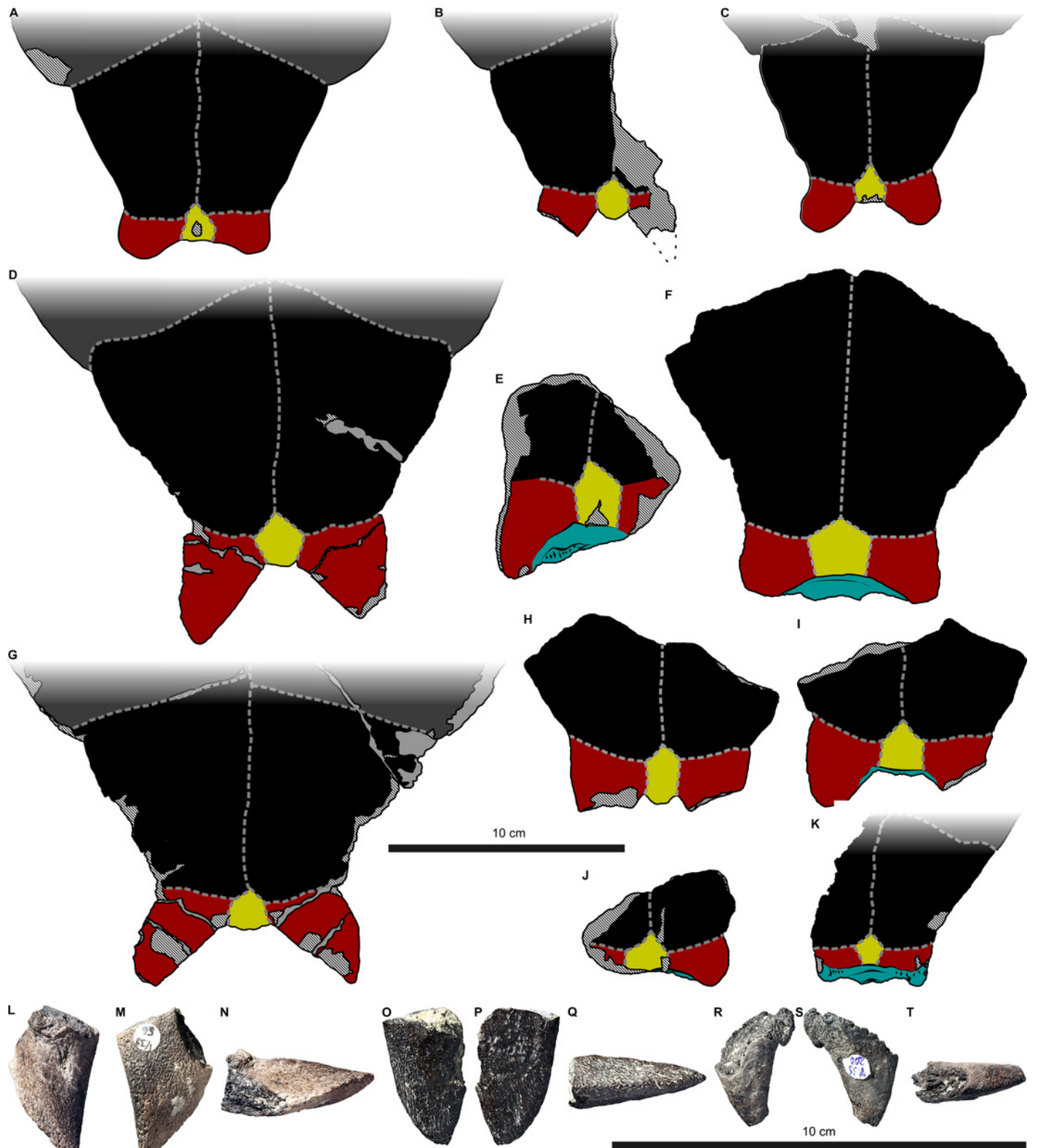
Figure 10

Results of the Principal Component Analysis of the caudal plastral region.

Principal Component Plots showing (A) the first against second and (B) the first against the third Principal Component of the caudal plastral region. The main shape changes for each PC are represented by wireframes, black wireframe is the average shape, while the red line represent shape changes connected to adequate PCs. Results of (C) regression analysis as an representation of the influence of log-transformed size on shape. *Proterochersis robusta* is represented by stars, *P. porebensis* by dots. Representations of scute shapes not to scale.

A

B

C
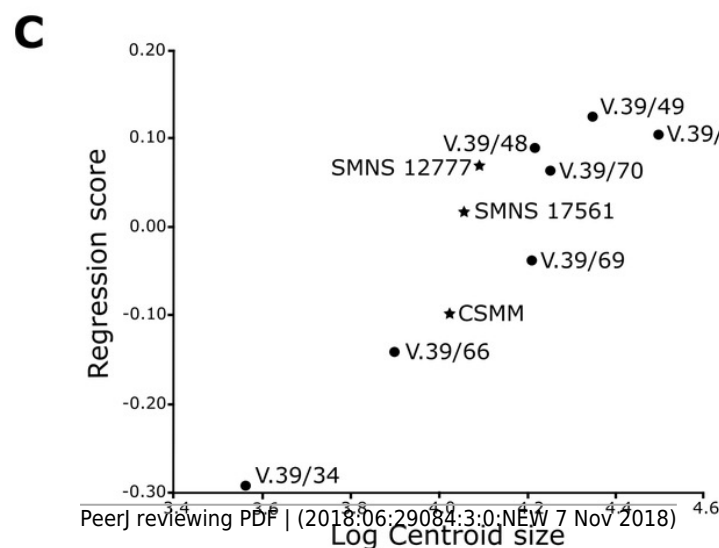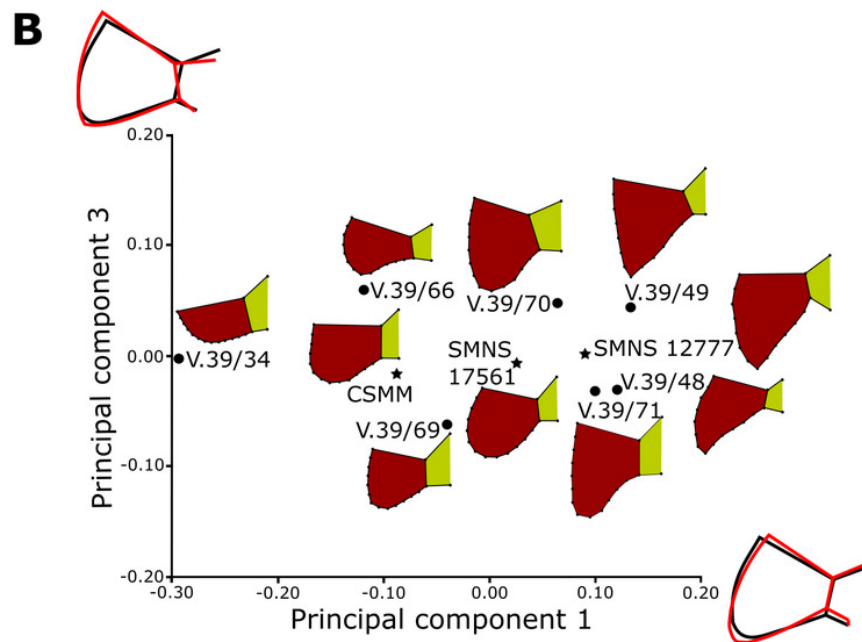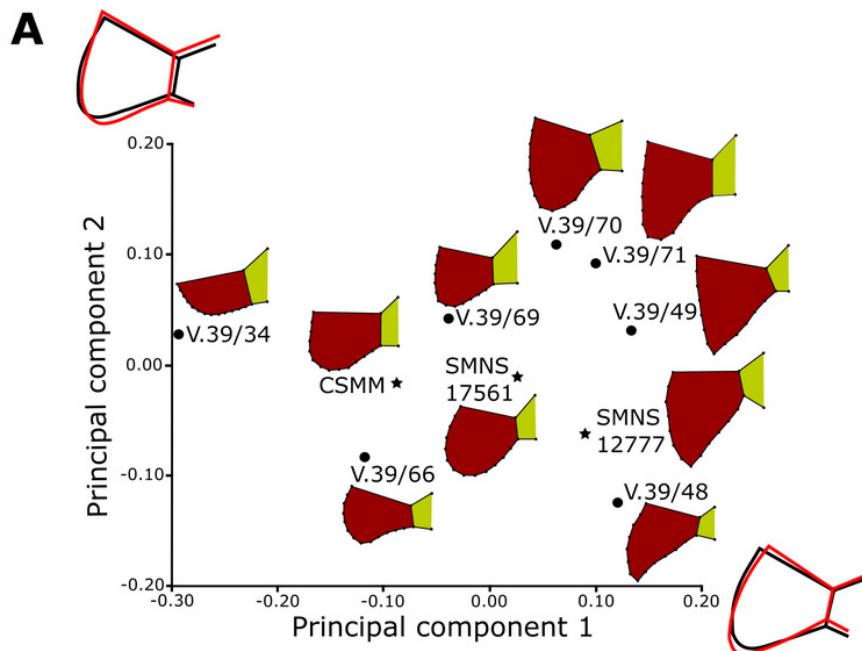
Definition of landmarks used in Principal Component Analyses.

1   Definition of landmarks used in Principal Component Analyses.

Plastron region	Plane	Landmark	Definition
Gular	Ventral	1	Caudal end of the intergular sulcus
		2	Caudal end of the sulcus between the gular and extragular scute
		3	Laterocaudal tip of the extragular scute
		12	Cranial end of the sulcus between the gular and extragular scute
		21	Cranial end of the intergular sulcus
	Vertical cross-section	1	Sulcus between the extragular and humeral scute
		15	Posterodorsal edge of the extragular scute
Anal	Ventral	1	Cranial tip of the intercaudal scute
		2	Caudal edge of the intercaudal scute
		3	Cranial end of the caudointercaudal sulcus
		4	Caudal end of the caudointercaudal sulcus
		17	Lateral end of the caudoanal sulcus